Author Manuscript

Author Manuscript

Author Manuscript

Author Manuscript

HHS Public Access

Author manuscript

Dev Cell. Author manuscript; available in PMC 2020 October 07.

Published in final edited form as:

Dev Cell. 2019 October 07; 51(1): 7–20.e6. doi:10.1016/j.devcel.2019.08.001.

Lysosome-rich enterocytes mediate protein absorption in the vertebrate gut

Jieun Park[1], **Daniel S. Levic**[1], **Kaelyn D. Sumigray**[2], **Jennifer Bagwell**[1], **Oznur Eroglu**[1], **Carina Block**[1], **Cagla Eroglu**[1], **Robert Barry**[3], **Colin R. Lickwar**[4], **John F. Rawls**[4], **Stephen A. Watts**[3], **Terry Lechler**[1,2], **Michel Bagnat**[1,5,*]

[1]Department of Cell Biology, Duke University, Durham, NC 27710, USA

[2]Department of Dermatology, Duke University Medical Center, Durham, NC 27710, USA

[3]Department of Biology, University of Alabama at Birmingham, Birmingham, AL 35294, USA

[4]Department of Molecular Genetics and Microbiology, Duke University, Durham, NC 27710, USA

[5]Lead Contact

SUMMARY

The guts of neonatal mammals and stomachless fish have a limited capacity for luminal protein digestion, which allows oral acquisition of antibodies and antigens. However, how dietary protein is absorbed during critical developmental stages when the gut is still immature is unknown. Here, we show that specialized intestinal cells, which we call lysosome-rich enterocytes (LREs), internalize dietary protein via receptor-mediated and fluid-phase endocytosis for intracellular digestion and trans-cellular transport. We identify a conserved endocytic machinery in LREs, composed of the scavenger receptor complex Cubilin/Amnionless and Dab2, that is required for protein uptake by LREs and for growth and survival of larval zebrafish. Moreover, impairing LRE function in suckling mice, via conditional deletion of Dab2, leads to stunted growth and severe protein malnutrition reminiscent of kwashiorkor, a devastating human malnutrition syndrome. These findings identify digestive functions and conserved molecular mechanisms in LREs that are crucial for vertebrate growth and survival.

Graphical Abstract

*Correspondence: michel.bagnat@duke.edu.

AUTHOR CONTRIBUTIONS

Conceptualization, M.B. and J.P.; Methodology, M.B. and J.P.; Investigation, J.P., D.S.L., K.D.S., C.B., O.E., and J.B.; Formal Analysis, C.R.L.; Resources, R.B., S.A.W., J.F.R., C.E., and T.L.; Writing – Original Draft, M.B. and J.P.; Writing – Review & Editing, M.B., J.P., D.S.L., T.L. and C.E.; Supervision, M.B.

Publisher's Disclaimer: This is a PDF file of an unedited manuscript that has been accepted for publication. As a service to our customers we are providing this early version of the manuscript. The manuscript will undergo copyediting, typesetting, and review of the resulting proof before it is published in its final citable form. Please note that during the production process errors may be discovered which could affect the content, and all legal disclaimers that apply to the journal pertain.

DECLARATION OF INTERESTS

Authors declare no competing interests.

Author Manuscript Author Manuscript Author Manuscript Author Manuscript

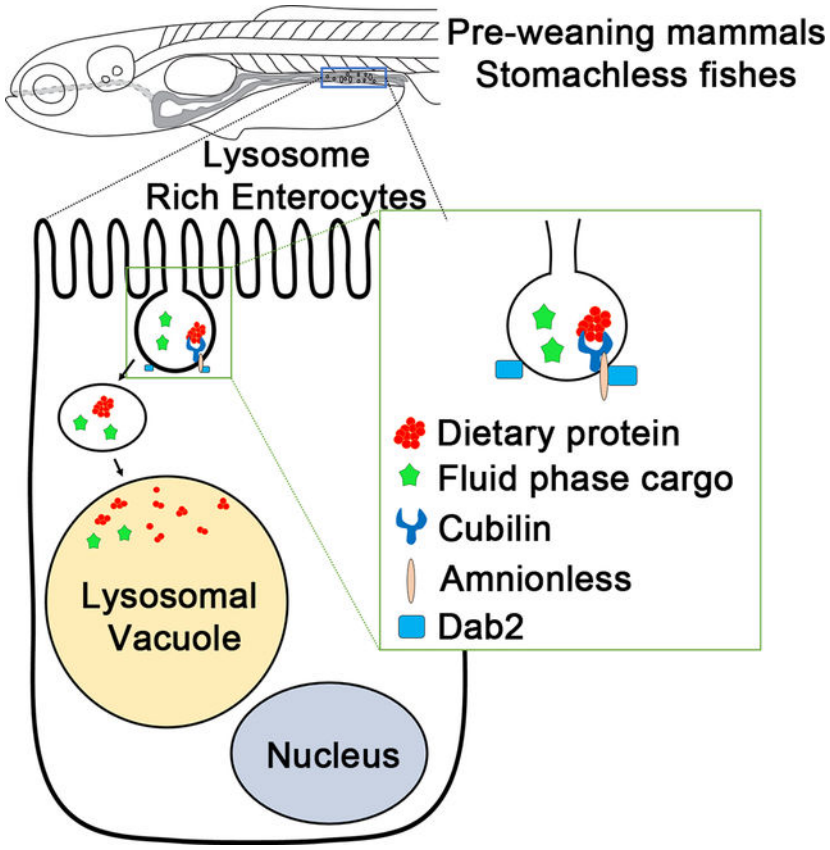

eTOC BLURB

Lysosome-rich enterocytes (LREs) are highly endocytic enterocytes found in pre-weaning mammals and stomachless fishes. Park et al. report that LREs mediate dietary protein absorption in the immature vertebrate gut via a multi-ligand endocytic machinery composed of Cubilin, Amnionless and Dab2, and a large lysosomal vacuole where dietary proteins are digested.

INTRODUCTION

Protein is an essential macronutrient for organismal growth and health. Protein digestion in weaned mammals occurs in the lumen of gastrointestinal (GI) tract by the action of pepsin in the stomach, followed by various proteases in the intestinal lumen. This produces oligopeptides and amino acids that are then taken up by enterocytes via specific transporters (Henning, 1985). By contrast, in the GI tract of zebrafish and suckling stage mammals, proteins are not fully digested in the lumen due to low protease activity (Henning, 1985; Robberecht et al., 1971; Rombout et al., 1985; Zhang et al., 2005). This allows antigens and maternal antibodies to be preserved and thus contribute to the development of innate and adaptive immune systems (Kulkarni and Newberry, 2019; Reinhardt, 1984). However, this feature of the immature vertebrate gut also presents a nutritional challenge and highlights the need for an alternative mechanism mediating dietary protein absorption. Despite its critical importance in organismal development and survival, how dietary protein absorption occurs in the immature vertebrate gut remains unclear.

Author Manuscript Author Manuscript Author Manuscript Author Manuscript

One possibility is that when the GI tract is still immature, dietary protein is internalized and digested intracellularly by intestinal epithelial cells. All eukaryotic cells internalize membrane, protein cargo and fluid from the extracellular medium. Some cargoes such as growth factors are recognized by specific receptors that enable their uptake (i.e. receptor-mediated endocytosis), while other proteins and soluble cargoes are simply internalized along with the fluid in a non-specific fashion (i.e. fluid-phase endocytosis). Fluid-phase endocytosis, also known as pinocytosis, can occur as a byproduct of receptor-mediated endocytosis or via endocytic pathways such as caveolae internalization and various forms of clathrin-independent endocytosis that are not fully understood (Johannes et al., 2015).

Classic tracing and electron microscopy (EM) experiments suggested that proteins present in the lumen of stomachless fish and immature mammalian GI tract can be internalized by a subpopulation of intestinal cells known as vacuolated enterocytes (Kleinman and Walker, 1984) via non-specific fluid-phase endocytosis and membrane adsorption (Gonnella and Neutra, 1984; Graney, 1968; Rombout et al., 1985). However, it is unclear if this activity is specific for proteins or sufficient in volume to be of nutritional importance.

Vacuolated enterocytes can be found in the ileum of pre-weaning mammals and the homologous intestinal region of zebrafish and other fishes (Harper et al., 2011; Kraehenbuhl and Campiche, 1969; Lickwar et al., 2017; Ng et al., 2005; Rodriguez-Fraticelli et al., 2015; Wallace et al., 2005). In mammals, vacuolated enterocytes are replaced by mature enterocytes at weaning and premature replacement results in growth retardation and elevated neonatal mortality (Harper et al., 2011; Muncan et al., 2011). In contrast, zebrafish vacuolated enterocytes persist into adulthood (Lickwar et al., 2017; Ng et al., 2005; Wang et al., 2010). Notably, previous work showed that reduction in the number and endocytic activity of vacuolated enterocytes, due to loss of Pllp function, impairs larval survival under nutrient limiting conditions (Rodriguez-Fraticelli et al., 2015). Together, these studies suggested that vacuolated enterocytes have an important function in zebrafish and pre-weaning mammals. However, whether vacuolated cells play a nutritional role, what types of nutrients they absorb, and what cellular mechanisms control their physiological activity are unknown.

Here, we used a comprehensive approach to elucidate the cellular and molecular mechanism mediating protein absorption in the immature gut of zebrafish and suckling mice. We show that vacuolated enterocytes, which we define as lysosome-rich enterocytes (LREs), preferentially internalize dietary proteins both via receptor-mediated and fluid-phase endocytosis and digest them intracellularly. We identify a multi-ligand endocytic machinery, composed of Cubilin (Cubn), Amnionless (Amn) and Dab2, that mediates the endocytic activity of LREs. Using custom diets and CRISPR/Cas9-generated mutants, we show that LRE-mediated protein absorption is crucial for larval zebrafish growth and survival. Conditional deletion of Dab2 in pre-weaning mice impairs protein absorption in LREs, leading to severe malnutrition and stunted growth, showing that LREs are morphologically and functionally conserved between zebrafish and suckling mammals.

Author Manuscript Author Manuscript Author Manuscript Author Manuscript

RESULTS

Luminal proteins are internalized and digested intracellularly by LREs in the zebrafish intestine.

To investigate the function of vacuolated enterocytes in the larval zebrafish, we gavaged animals with fluorescent dextran (fDex) (Cocchiaro and Rawls, 2013). After gavage, we observed a population of cells in the posterior mid-intestine that avidly internalize fDex and found that these cells express high levels of the lysosomal marker Lamp2 and possess a large supranuclear vacuolar system (Figures 1A–1C). This is in contrast to other intestinal epithelial cells (IECs) that have smaller lysosomes scattered throughout the cell (Figure 1B). We therefore named these vacuolated intestinal cells lysosome rich enterocytes (LREs).

To define the luminal contents internalized by LREs, we gavaged 6 days post fertilization (dpf) larvae with a mixture of purified mCherry (Shaner et al., 2004) protein and fluorescently labeled fatty acid (Semova et al., 2012) and imaged cargo uptake throughout the entire gut after one hour using live confocal microscopy. We observed that while both fluorescent cargoes were present along the length of the lumen, LREs internalized mCherry but not fatty acids, which were instead absorbed by IECs in the anterior gut as previously shown (Carten et al., 2011) (Figure 1D). We confirmed that the vacuolar compartments in LREs were *bona fide* lysosomes by labeling experiments with the acidotropic dye Lysotracker (Figure 1E). Moreover, the vacuole membranes were lined by GFP-Rab32a, which is also found at the membrane of notochord vacuoles, a large lysosome related organelle (Ellis et al., 2013) (Figure 1E).

Following gavage, mCherry was rapidly internalized from the lumen into apical endosomes and late endosomes (Figure 1F, arrowheads and Figures S1A–S1E), accumulating progressively in vacuoles (Figure 1F, arrows). To investigate the kinetics of this process, we gavaged mCherry or mTurquoise, whose fluorescence is pH insensitive (Shinoda et al., 2018), and measured their accumulation within lysosomal vacuoles, lined by GFP-Rab32a, relative to total cellular signal (Cv/Cc) over time. mCherry and mTurquoise reached their half maximal saturation within 2.6 ± 0.2 hours and 0.8 ± 0.2 hours, respectively, and subsequently reached an equilibrium between their rate of import from the luminal pool and their degradation in the vacuole (Figure 1G). To assess the degradation rate of each protein in LREs, we gavaged mCherry or mTurquoise and allowed their uptake for one hour. Then, we flushed the luminal protein pool by gavaging PBS and measured the fluorescence intensity of each protein in LREs over time. While mTurquoise was quickly degraded (0.23 hours half-life) and was essentially gone by 2 hours post-flushing, mCherry had a much longer half-life (2.7 hours) and was detectable in LREs 5 hours post-flushing, which is consistent with the relative resistance to proteolysis reported for mCherry (Shinoda et al., 2018) (Figure 1H). These data show that LREs continuously internalize proteins from the lumen and digest them intracellularly.

To assess internalization of labeled cargoes by LREs, we first gavaged mCherry and the water-soluble and small molecular weight cargo lucifer yellow (LY) (Swanson et al., 1985) into two transgenic fish lines that allow visualization of the apical membrane (Figures S1F–S1K). We quantified mCherry and LY uptake in LREs and found that both were efficiently

Author Manuscript Author Manuscript Author Manuscript Author Manuscript

internalized by these cells. However, the peaks of absorption were slightly shifted, with mCherry concentrated at the anterior LRE segment (Figures 1I and 1J). When we analyzed mCherry internalization using increasing concentrations of the protein, we found that its uptake profile shifted to the posterior of the LRE region, similar to LY, suggesting that mCherry absorption in anterior LREs is saturatable (Figure 1K). Additional experiments using other pH insensitive protein cargoes revealed distinct internalization profiles for each protein (Figures 1L and S2A). When we gavaged mCherry together with an excess of mTurquoise, uptake of mCherry was impaired (Figure 1M) and *vice versa* (Figure S2D), suggesting competition for the same internalization machinery. Similar results were obtained using mCherry and labeled transferrin (Figures S2B and S2C). These data suggest that protein uptake in LREs is mediated by a saturable mechanism of broad specificity and variable affinity, as the internalization peaks are slightly different for each protein we tested. We also found that a fraction of internalized fluorescent proteins and LY was later found in the pronephros (kidney), liver and gall bladder (Figures S3A and S3B), suggesting that one function of LREs is to mediate transcellular transport of proteins and soluble cargoes across the intestinal barrier and subsequently to other tissues.

LREs specifically express a multiligand endocytic machinery composed of Cubn, Amn and Dab2.

To identify the molecular mechanisms mediating protein uptake in LREs, we gavaged fDex into 5 dpf *TgBAC(cldn15la-GFP)* transgenic larvae in which Cldn15la-GFP localizes to the lateral surface of all intestinal cells (Alvers et al., 2014). IECs (GFP only) and LREs (GFP +fDex) were isolated using florescence-activated cell sorting (FACS) 24 hours after gavage (Figures 2A and S4A). Following RNAseq analyses, we found that LREs showed increased expression of *pllp* and *lamp2*, consistent with previous results (Rodriguez-Fraticelli et al., 2015), and reduced expression of IEC markers such as *ifabp2* and *mttp* (Figures 2B and S4B). Differential expression analysis, cluster dendrogram, and principal-component analysis confirmed that each population had unique enrichment signatures (Figures S4C–S4E). Profiling using Gene Ontology (GO) terms and Kyoto Encyclopedia of Genes and Genomes (KEGG) pathway analysis revealed that the terms associated with lysosomal activity including lysosome, proteolysis and peptidase activity were highly enriched in LREs (Figure S4F), which is consistent with the presence of a prominent lysosomal degradative system in these cells. Among the most highly enriched LRE transcripts were *cubilin* (*cubn*), *amnionless* (*amn*) and *dab2* (Figure 2B).

Cubn is a large, broad spectrum scavenger receptor previously shown to be involved in protein retrieval in the kidney and absorption of intrinsic factor-vitamin B12 in the intestine (Amsellem et al., 2010; Nielsen et al., 2016). In the mouse embryonic visceral yolk sac endoderm, Cubn has also been implicated in the absorption of nutrients including folic acid, transferrin, retinoic acid and cholesterol (Kozyraki and Gofflot, 2007; Zohn and Sarkar, 2010). Amn forms a large complex with Cubn (Larsen et al., 2018), where Amn functions as a transmembrane link for Cubn and provides intracellular binding sites for the endocytic adaptor Dab2 (Fyfe et al., 2004; He et al., 2005; Maurer and Cooper, 2005; Strope et al., 2004) (Figure 2C). In situ hybridization for the respective transcripts revealed that *cubn, amn* and *dab2* are expressed in a highly specific manner in the LRE region of the gut and in

Author Manuscript Author Manuscript Author Manuscript Author Manuscript

the pronephros (Figure 2D). In contrast, *lrp2a* (a.k.a megalin), which encodes another scavenger receptor, was undetectable in LREs by in situ hybridization and instead showed specific expression in the pronephros (Figures 2D, S5A and S5B). Together, these data suggest that Cubn/Amn and Dab2 mediates saturable uptake of proteins in LREs.

The Cubn/Amn endocytic receptor complex mediates protein uptake in LREs.

To test the role of Cubn in LRE protein uptake, we generated a mutant zebrafish line using CRISPR/Cas9 (Figures S5C–S5E) and monitored mCherry/LY uptake as before. Interestingly, while mCherry uptake was significantly impaired, LY internalization was unaffected in *cubn* mutants (Figures 3A and 3B). Similar results were obtained using mTurquoise and transferrin (tfn) as protein cargoes (Figure S2E), suggesting Cubn mediates the uptake of a broad spectrum of proteins, but not small soluble compounds such as LY. The residual (~20%) uptake of tfn remaining in *cubn* mutants (Figure S2E, asterisk) was likely mediated by its cognate receptor, the tfn receptor, which is expressed in LREs according to our RNAseq data. To test if Cubn function depends on Amn as shown in other contexts (Fyfe et al., 2004; He et al., 2005), we also generated *amn* mutants (Figures S5F–S5H) and assayed LRE activity. mCherry, but not LY, uptake was significantly impaired upon loss of Amn function (Figure 3C). These data indicate that protein uptake in LREs is largely mediated by the Cubn/Amn complex in zebrafish.

Dab2 mediates fluid-phase and receptor-dependent endocytosis in LREs.

To test the role of Dab2 in cargo uptake from the intestinal lumen, we first isolated the phosphotyrosine binding (PTB) domain of Dab2, which acts as a dominant negative (DN) (Mishra et al., 2002), and expressed it mosaically in the intestine under the control of QUAS (Subedi et al., 2014), using *cldn15la:QF2* as a driver (Figure 4A). Using fDex and mCherry as cargoes, we found that uptake was impaired in cells expressing DN-Dab2 in a cell autonomous manner (Figures 4B and 4C). We then generated a *dab2* zebrafish mutant using CRISPR/Cas9 (Figures S5I–S5K) and assayed mCherry/LY uptake, confirming that uptake of both receptor-dependent and fluid-phase cargoes in LREs require Dab2 function (Figures 4D and 4E). Thus, Dab2 function is critical for the robust ability of LREs to internalize protein and other soluble cargoes. In contrast to protein and other soluble cargo uptake, fatty acid uptake in IECs was unaffected by loss of Cubn/Amn or Dab2 function (Figures S6A–S6D). We also examined lysosomal vacuole formation in LREs and found that it occurs normally upon loss of Cubn/Amn or Dab2 function (Figures S6E–S6F), indicating that formation of the large lysosomal compartment of LREs is not dependent on their internalization activity.

Loss of LRE protein uptake impairs growth and survival in larval zebrafish.

Our data indicate that protein uptake in the zebrafish intestine occurs via the Cubn/Amn receptor complex, which is internalized via the Dab2 endocytic adaptor. Our data also indicate that fluid-phase endocytosis is dependent on the activity of the Dab2 adaptor but not on Cubn/Amn receptor complex. In previous work we found that loss of Pllp, which interacts with Dab2 in MDCK cells (Rodriguez-Fraticelli et al., 2015), partially impairs LRE differentiation and reduces larval survival under nutrient limiting conditions (Rodriguez-Fraticelli et al., 2015). Thus, we investigated whether LREs play a role in dietary protein

Author Manuscript Author Manuscript Author Manuscript Author Manuscript

absorption in zebrafish. First, we generated nearly isocaloric custom diets with high protein (HP) or low protein (LP) content. Then, we raised *cubn* and *dab2* mutant and their heterozygous control larvae under a calorie-restricted HP or LP feeding regime as well as a non-calorie-restricted standard control feeding regime. Under those conditions, *cubn* mutants survived normally when fed a standard control diet or a calorie-restricted HP diet, but showed poorer survival rate under a calorie-restricted LP diet (Figure 5A). On the other hand, *dab2* mutants presented a sharp and significant reduction in survival relative to their heterozygous controls under all feeding conditions (Figure 5B). We also found that both *cubn* and *dab2* mutants fed a standard control diet were growth-stunted (Figure 5C), due to poor growth during larval stages (Figure 5D). In addition to strong survival and growth defects, *dab2* mutants presented a poorly folded and shorter, but well polarized epithelium compared to heterozygous controls (Figure 5E), which is typically observed in starved larvae.

To test whether growth and survival defects we observed were in part due to essential functions of renally expressed *cubn*, we examined LRE protein uptake, larval survival and body length in *lrp2a* mutants, which exhibit kidney filtration defects (Anzenberger et al., 2006; Nielsen et al., 2016; Veth et al., 2011). Internalization of Cubn, which lacks transmembrane domain, relies on both Megalin (Lrp2a) and Amn in this tissue and loss of Lrp2a function also leads to loss of Cubn function in the pronephros (Ahuja et al., 2008; Christensen and Nielsen, 2007). By contrast with *cubn* and *dab2* mutants, we found that *lrp2a* mutants had no mCherry or LY uptake defects, nor survival or growth defects with respect to controls (Figure 6), indicating that *lrp2a* mutants have normal LRE function. These data suggest that the survival defects observed in *cubn* and *dab2* mutants are likely not due to impaired kidney function. Together, these data reveal that protein uptake in LREs is required for normal larval growth and survival in zebrafish. We postulate that the reduced survival of *dab2* with respect to *cubn* mutants is due to the fact that both receptor-mediated and fluid-phase endocytosis of proteins are impaired. Alternatively, it is also possible that other essential soluble factors are also absorbed via LREs.

Loss of LRE function results in growth stunting and intestinal swelling in suckling mice.

Classic EM and protein uptake experiments suggest that intestinal LREs present in suckling stage mammals are involved in the uptake of milk components (Gonnella and Neutra, 1984; Kraehenbuhl and Campiche, 1969). Proteome data also showed that Cubn and Dab2 are expressed in the ileum of suckling mice and rats (Vazquez-Carretero et al., 2014). We therefore investigated whether LREs are functionally conserved between zebrafish and mice. We first examined mCherry uptake *ex vivo* using ileal segments harvested from P7 suckling mice and observed robust uptake of the protein in cells that closely resemble zebrafish LREs morphologically (Figures 7A and 7B). By contrast, mCherry internalization in duodenum IECs was limited to small vesicular structures (Figure 7G, arrowheads). We also found that P7 mouse ileal enterocytes express high levels of Lamp2, labeling large supranuclear compartments similar to those of zebrafish LREs (Figures 7C and 7D). In contrast, IECs in more anterior intestinal segments of both mice and zebrafish showed Lamp2 localization to small puncta (Figures 7E and 7F). These data indicate that LREs are present in the ileum of

Author Manuscript Author Manuscript Author Manuscript Author Manuscript

suckling stage mice and share the same morphology, marker expression and activity with zebrafish LREs.

Given our finding that Dab2 is essential for LRE function in zebrafish, we next examined its expression in the ileum of pre-weaning mice. We found that mouse Dab2 is highly enriched in LREs, where it localizes to the subapical domain (Figure 7H). Interestingly, in mammals LREs are present transiently and then replaced at weaning by regular enterocytes (Muncan et al., 2011). We next analyzed previously published ileum transcriptome data (Schjoldager et al., 2008) and found that this developmental transition is associated with a sharp downregulation of ileal Dab2. To define the function of Dab2-expressing LREs in mice, we used a previously developed conditional Dab2 null allele ($Dab2^{(fl/fl)}$) (Morris et al., 2002) combined with a Villin-Cre (Madison et al., 2002) transgene to generate an intestine-specific conditional knockout (cKO). Similar to our results with zebrafish, we found that loss of Dab2 completely abrogated mCherry uptake in mouse LREs but did not affect Lamp2 expression or vacuole morphology (Figure 7I). These data indicate that LREs are functionally conserved between zebrafish and mice.

We then monitored the weight and growth of Dab2 cKO mice until weaning (Postnatal day (P) 21-P22) and found they present significant growth defects in comparison to their sex-matched WT littermates (Figures 7J–7M). Interestingly, a prominent swelling of the GI tract was observed in a large fraction (11 out of 13, $p<0.05$) of cKO animals that appeared to result from submucosal edema (Figures 7N–7R). On the other hand, differentiation of goblet cells and crypt morphology were not affected (Figure 7R). Thus, Dab2 has conserved functions in vertebrate LREs. Collectively, our data reveal that LREs are a highly conserved intestinal cell type that plays an essential nutritional role in the early vertebrate gut and are critical for normal development.

DISCUSSION

Here, we have elucidated the mechanism by which dietary protein is absorbed in the immature gut of zebrafish and suckling mice. We found that a specialized population of intestinal cells we define as lysosome-rich enterocytes (LREs), internalize luminal proteins via fluid-phase and receptor-mediated endocytosis and digest them intracellularly. We show that uptake and internalization of dietary protein is mediated by a receptor complex composed of Cubn, Amn and the endocytic adaptor Dab2. This molecular machinery is required for LRE function and for growth and survival of larval zebrafish. Importantly, we found that LREs are highly conserved at the morphological and functional level between mouse and zebrafish. Taken together, our results reveal a fundamental and highly conserved cellular mechanism underlying protein absorption in the immature vertebrate gut.

LREs are specialized intestinal epithelial cells that mediate dietary protein absorption.

Histological analyses detected the presence of highly vacuolated enterocytes in the intestine of multiple vertebrate species of mammals and fish (Asari et al., 1987; Trahair and Robinson, 1989; Wallace et al., 2005; Wilson et al., 1991; Zabielski et al., 2008). Tracing of proteins by EM led to the notion that vacuolated enterocytes play a nutritional role by participating in the digestion of milk nutrients via non-selective fluid-phase endocytosis and

Author Manuscript Author Manuscript Author Manuscript Author Manuscript

membrane adsorption (Gonnella and Neutra, 1984; Graney, 1968). However, the validity of these assumptions could not be truly tested due to the lack of understanding of the cellular and molecular mechanisms that control the functions of these cells. Here, we show that, contrary to what was previously proposed, zebrafish LREs specifically internalize proteins from the intestinal lumen via receptor-mediated endocytosis. We found that the multi-ligand receptor Cubilin (Cubn) mediates dietary protein internalization (Figures 1I–1M, 3 and S2). Using live imaging in zebrafish, we were able to directly visualize protein uptake, intracellular transport and degradation in LRE vacuoles, which we found to be large lysosomes (Figures 1F–1H). Our studies revealed that LREs have an astounding endocytic and digestive activity that allows them to virtually function as a digestive organ. This striking specialization is reflected at the gene expression level with the upregulation of the lysosomal machinery, particularly of digestive proteases, in LREs respect to other intestinal cells (Figure S4F). The physiological function of LREs requires that these cells develop a giant lysosomal vacuole, which allows intracellular digestion of internalized proteins. Interestingly, the formation of the lysosomal vacuole was not dependent on the protein internalization activity of these cells (Figures S6E–S6F), indicating the existence of other molecular mechanism that control the specialization of LRE vacuoles.

In zebrafish LREs persist through adulthood (Lickwar et al., 2017; Ng et al., 2005; Wallace et al., 2005); whereas, in mammals they are replaced with adult enterocytes as the intestinal epithelium undergoes major structural and biochemical changes during the suckling to weaning transition (Harper et al., 2011; Muncan et al., 2011). Comparison of our gene expression data with that of adult zebrafish intestine (Wang et al., 2010) revealed that a number of LRE-enriched genes remain enriched in the homologous region (segment 5) of the adult zebrafish intestine (Figure S7C), which is consistent with a persistence of highly endocytic LREs we observed in adult zebrafish (Figures S7D and S7E). However, future work will be needed to determine whether LREs continue to play a major nutritional role in adult zebrafish.

In contrast to zebrafish, comparison of our gene expression data with that of pre-weaning and post-weaning mouse ileum (Schjoldager et al., 2008) revealed that lysosome and LRE-enriched genes are downregulated in mice after weaning (Figures S7A and S7B). The transition that occurs during weaning in mammals is associated with the change in the expression of the transcriptional repressor *Blimp1* ((Harper et al., 2011; Muncan et al., 2011). It will be interesting to investigate whether the differentiation of LREs and the mechanisms controlling the expression of the cellular and molecular machinery that characterizes these cells is conserved between zebrafish and mammals.

LREs utilize the Cubn/Amn scavenger receptor complex and the Dab2 adaptor for protein uptake.

LREs are remarkably active and effective in retrieving proteins from the intestinal lumen. This is made possible by the activity of the broad-spectrum receptor Cubn. The use of receptor-mediated endocytosis provides a concentrating mechanism that allows efficient protein absorption even when dietary protein is not abundant. While each protein internalized by LREs exhibited distinct uptake profiles (Figures 1J, 1L, and S2A), we also

Author Manuscript Author Manuscript Author Manuscript Author Manuscript

found evidence of competition between protein cargoes (Figures 1M and S2B–S2D), suggesting that Cubn recognizes a general protein feature with variable affinity. Alternatively, each protein might have a different number of epitopes recognized by Cubn. The survival of *dab2* zebrafish mutants was more severely compromised compared to that of *cubn* mutants in all feeding regimes (Figure 5B), likely due to the fact that Dab2 is involved in both fluid-phase and receptor-mediated endocytosis (Figure 4). This suggests that sufficient absorption of dietary proteins needs both fluid-phase and receptor-mediated endocytosis. Alternatively, some of the non-protein soluble cargoes, internalized via the fluid-phase endocytosis in LREs, might be essential for larval survival and growth.

Replacement of LREs by regular enterocytes in mice correlates with weaning and coincides with a significant reduction in the expression of *Dab2* (Schjoldager et al., 2008) (Figures S7A and S7B), suggesting Dab2 function determines the endocytic capacity of intestinal cells. However, ectopic expression of Dab2 in enterocytes did not enhance their protein uptake capacity (data not shown). Identification of co-regulated genes that are differentially expressed in LREs versus other IECs may reveal the core genetic program driving LRE physiology.

Systemic roles of LREs in health and disease

We found that LREs are remarkably conserved between zebrafish and mice. At the functional level, this is reflected in their core nutritional function, which allows efficient protein absorption via a conserved molecular machinery. The conserved function of LREs may also extend to their role in transcellular transport, which allows the passage of intact proteins and other soluble cargoes across the intestinal barrier (Figure S3). In zebrafish, while most cargoes internalized by LREs are destined to lysosomal vacuole where they are digested, some of the cargoes undergo trans-cellular transport across LREs and accumulate in extra-intestinal tissues over time (Figure S3). Similarly, in neonatal mammals, transport of antibodies and luminal antigens across intestinal epithelium is highly active (Buchanan et al., 2012; Turfkruyer et al., 2016). This phenomenon has been attributed to the presence of an immature intestinal permeability barrier. However, our results indicate that in zebrafish, LREs and their Cubn/Amn/Dab2 machinery provide a major route for trans-epithelial transport (Figures S3C and S3D), suggesting that LREs are also likely responsible for the high transcellular permeability of the mammalian neonatal intestine. This conserved activity may provide a high-capacity route for transcellular transports of intact proteins like antibodies and other soluble antigens including bio-active microbial products (Hill et al., 2016). We speculate that LREs may thus facilitate passive immunity in mammals, as well as the development of the innate immune system, tolerance to food and microbial antigens, and host-microbe communication in vertebrates.

Interestingly, we found that both Tfeb and Slc39a8, which are components of the mTORC1 pathway (Rebsamen et al., 2015), are highly upregulated in LREs compared to IECs (not shown). While this may simply reflect the abundance of lysosomes in LREs, it is tempting to speculate that LREs may sense the availability of dietary nutrients. Since LREs internalize dietary proteins and digest them intracellularly, the level of amino acids within the lysosomal vacuole should reflect dietary nutrient availability.

Author Manuscript Author Manuscript Author Manuscript Author Manuscript

Our mouse data show that loss of *Dab2* in the intestine leads to growth stunting and intestinal swelling, which is reminiscent of kwashiorkor. Kwashiorkor is a disease caused by severe protein malnutrition and is characterized by the presence of oedema, dermatosis, and diarrhea (Golden, 1998; Williams et al., 2003). The origin of kwashiorkor has been debated and remains poorly understood, and potential causes of the disease include low plasma albumin, low protein uptake, microbiota disturbances (Coulthard, 2015; Smith et al., 2013b). While our data supports low protein uptake as a leading cause of kwashiorkor, it is also possible that insufficient LRE protein uptake in *Dab2* cKO mice leads to an alteration in their gut microbiota, which in turn may cause intestinal swelling. Indeed, earlier gnotobiotic experiments in zebrafish suggest that LRE function is regulated by host-microbe interactions (Bates et al., 2006; Rawls et al., 2004). Therefore, it is possible that a dysbiosis of environmental origin may lead to a loss of LRE activity that would in turn cause protein malabsorption. Further investigation of this mouse model may provide insights into the effects of perinatal protein malnutrition in humans.

In conclusion, our work shows an important physiological role for LREs that is remarkably conserved at the molecular and functional level between zebrafish and mice. Future research of the biology of LREs has the potential to illuminate how vertebrate animals interact with the environment as they develop and mature.

STAR ★ METHODS

LEAD CONTACT AND MATERIALS AVAILABILITY

Further information and requests for resources and reagents should be directed to and will be fulfilled by the Lead contact, Michel Bagnat (michel.bagnat@duke.edu). Zebrafish lines, plasmids and other reagents generated in the study will be available upon request.

EXPERIMENTAL MODELS AND SUBJECT DETAILS

Fish—All fish were used in accordance with the Duke University Institutional Animal Care and Use Committee (IACUC) guidelines. Zebrafish (*Danio rerio*) stocks were maintained at 28°C in a recirculating system and bred by putting a male and a female zebrafish in a mating tank and controlling the day-night cycle (Westerfield, 2000). Genotypes were determined by fin clipping. Male and female breeders from 3–9 months of age were used to generate fish for all experiments. 5–30 dpf zebrafish larvae from the Ekkwill (EK) or AB/TL background were used in this study. No test on the influence of sex were performed as sex determination in zebrafish occurs in late juvenile stage, well after our experimental window. Strains generated for this study: *cubn*^{pd1169}, *dab2*^{pd1162}, *amn*^{pd1189}, *Tg(cldn15la:QF2)*^{pd1142}, *Tg(QUAS:GFP-Rab32a)*^{pd1201}, *Tg(QUAS:mCherry-snx27a)*^{pd1177} *Tg(hsp:laGFP)*^{pd1205}, *Tg(2.3k ifabp:sNgly-RFP)*^{pd1206}. Previously published strains: *lrp2a*^{mw1} (Veth et al., 2011), *TgBAC(cldn15la-GFP)*^{pd1034} (Alvers et al., 2014), *TgBAC(lamp2-RFP)*^{pd1044} (Rodriguez-Fraticelli et al., 2015), *TgBAC(anxa2b-RFP)*^{pd1113} (Marjoram et al., 2015), *Tg(hsp:Venus-FYVE)*^{pd1046} (Ellis et al., 2013).

Mice—All mice were used in accordance with the Duke University Institutional Animal Care and Use Committee (IACUC) and the Duke Division of Laboratory Animal Resources

Author Manuscript Author Manuscript Author Manuscript Author Manuscript

(DLAR) oversight. The Dab2 floxed (Morris et al., 2002) (B6;129S4-*Dab2*^{tm1Cpr}/J; Cat# JAX:022837; RRID: IMSR_JAX:022837) line was obtained through Jackson Laboratory. The Dab2 floxed mice were crossed to Villin-Cre (el Marjou et al., 2004) mice to generate intestinal epithelial-specific Dab2 conditional knockout (cKO) mice. Mice were genotyped by PCR, and both males and females were analyzed. Age and sex-matched pairs were selected for the paired comparison of WT and cKO mice as shown in Table S2. No test was performed to determine the influence of sex as no obvious differences were found. Mice were maintained in a barrier facility with 12-hour light/dark cycles. Mice had access to water and food *ad libitum*. The weight of Dab2 WT and Dab2 cKO mice were measured every three days from P0 to P22. At P22, the weight and length of mice were measured, and the intestine was dissected after sacrifice for further analysis. Intestinal length was measured, as was the diameter of the duodenum.

METHOD DETAILS

Genome Editing—Mutant lines were generated using CRISPR/Cas9. Guide RNA (gRNA) target sites were identified using CRISPRscan (Moreno-Mateos et al., 2015) and gRNAs were synthesized using the oligo-based method (Yin et al., 2015). *cubn*^{pd1169} mutants were generated using a gRNA targeting exon 5, *dab2*^{pd1162} mutants at exon 5, and *amn*^{pd1189} mutants at exon 1. gRNA target sequences were: cubn- 5’ TGTGAATGAGTGTCAGGTGT 3’, dab2– 5’ TGATGTTCAAGATGCAAGAG 3’, amn- 5’ GGGTTTACTGTGCGAGAAGG 3’. Zebrafish embryos were injected at the one cell stage with 150 pg/nl of Cas9 mRNA and 50 pg/nl of gRNA. Genotyping for *cubn* was performed using primers: forward, 5’ ACTCTGTTCACCTGCAGTGC 3’; (DCAPS primer (Neff et al., 1998)) reverse, 5’ TGACATCCGAGTGGAGTTCCTGCCAAGAC 3’. PCR products were then digested with HinfI enzyme for genotyping. Genotyping for *dab2* was performed using primers: forward, 5’ ACAGACGAGTTCCTCTTGGC 3’; reverse, 5’ CCGCTTCTTGCAGTGCTAGA 3’. Genotyping for *amn* was performed using primers: forward, 5’ GGATGAGCTTGCCTGTGGAT 3’; reverse, 5’ GAATGAGGTGGCGTCTCGAA 3’.

Transgenesis—All constructs for transgenic fish were generated using the Tol2kit gateway cloning system using the p5E-QF2, p5E-cldn15la, pME-QF2, pME-DN-Dab2, p3E-polyA, p3E-p2A-eGFP, and pDestTol2CG2 vectors (Kwan et al., 2007; Ellis et al., 2013). The p5E-QUAS and pME-QF2 vectors were gifts from Marnie Halpern (Subedi et al., 2014). The p5E-cldn15la vector was a gift from John Rawls (Murdoch et al., 2019). To generate pME-DN-Dab2, we amplified the PTB domain of Dab2, which acts as a dominant negative (Mishra et al., 2002). DN-Dab2 was amplified using the following primers: forward, 5’ CCACTCACCATGACTGCACCCGTGACCAG 3’; reverse, 5’ CTTTTGTCCAGCCTCCTGCTC 3’.

Soluble Fluorescent Protein Production—pRSET-mCherry and pRSETB–mTurquoise vectors were gifts from Kalina Hristova. mCherry and mTurquoise soluble fluorescent proteins were produced by uninduced expression in the BL21-Gold (DE3) strain of Escherichia coli. The fluorescent proteins were purified from the pellet of large bacterial culture using the His tag (Sarabipour et al., 2014).

Author Manuscript Author Manuscript Author Manuscript Author Manuscript

Gavage—5–6 dpf larvae were gavaged with 4 nl of 1.25 mg/ml mixture of Lucifer Yellow (ThermoFisher Scientific), Alexa Fluor 488 conjugated transferrin (ThermoFisher Scientific), Alexa Fluor 568 Dextran (ThermoFisher Scientific), Lysotracker (ThermoFisher Scientific), mCherry or mTurquoise for different gavage experiments using a previously described gavage technique (Cocchiaro and Rawls, 2013). In brief, the gavage technique is performed with a microforged needle which goes through the zebrafish larvae mouth and esophagus to directly inject the injection mixture into the gut lumen of zebrafish larvae. For protein competition assays (Figures 1M and S2B–S2D), higher concentrations of proteins were used (Indicated in the graphs). Gavaged larvae were imaged 4–5 hours after gavage using a Fluoview FV3000 (Olympus) confocal microscope. For lipid and protein uptake assays (Figures 1D and S6), 5 μl of 10 mg/ml BODIPY™ FL C16 (ThremoFisher Scientific) was air dried and dissolved in 5 μl of 100% EtOH. Then 50 μl of 5% egg yolk solution was added to make 1 mg/ml BODIPY™ FL C16 solution. 3 μl of 1 mg/ml BODIPY™ FL C16 solution and 1 μl 5 mg/ml mCherry solution were mixed to make the final concentration of BODIPY™ FL C16 and mCherry in the mixture to be 0.75 mg/ml and 1.25 mg/ml, respectively. Larvae were gavaged with 4 nl of the mixture and imaged after 1 hour using a Fluoview FV3000 (Olympus) confocal microscope.

Quantification of Relative Uptake by LREs—To quantify the relative amount of uptake along the length of LREs, images of LREs were analyzed with ImageJ software (NIH) using the “Plot Profile” function to obtain gray value along the length (pixel) of the image. Then, pixels were converted to μm and the gray values were used to calculate relative uptake of fluorescent cargoes. To visualize gavaged cargoes accumulation inside the lumen (Figures S1G, S1H, S1J and S1K), a line was drawn on optical sections of LRE confocal images and a line scan was performed using ImageJ. For kinetic analysis of mCherry or mTurquoise uptake over time (Figure 1G), 5 dpf larvae were gavaged with 4 nl of 1.25 mg/ml mCherry or mTurquoise and then fixed in 4% paraformaldehyde (PFA) at the indicated timepoints. Whole larvae were mounted on glass bottom dishes and LREs were imaged using confocal microscopy. Mean pixel intensity measurements of the vacuole (delimited by GFP-Rab32) and the whole cell were taken with ImageJ, and ratios of the two values for individual cells were plotted and analyzed using Graphpad Prism (GraphPad Software). For kinetic analysis of mCherry or mTurquoise degradation (Figure 1H), 5 dpf larvae were gavaged with 4 nl of 1.25 mg/ml mCherry or 5 mg/ml mTurquoise and incubated at 28°C for one hour to allow protein uptake by LREs. Then, the larvae were gavaged again with PBS to flush the remaining luminal protein pool. Then, larvae were fixed in 4% PFA at the indicated timepoints and LREs were imaged using confocal microcospy. Mean pixel intensity measurements of anterior LREs were taken with ImageJ and used to calculate relative fluorescence intensity. The values were plotted and analyzed using Graphpad Prism.

Cell Isolation and RNA Sequencing—For isolating IECs and LREs, 5 dpf *TgBAC(cldn15la-GFP)*^{pd1034} fish were gavaged with 1–2 nl of 2.5 mg/ml Alexa Fluor 568-Dextran, incubated at 28°C for 24 hours. Then, larvae were dissociated to generate single-cell suspensions for FACS by incubating in 0.25% trypsin-EDTA (Life Technologies) and 1% collagenase (Sigma-Aldrich) at 28°C for approximately 1.5 hr. Dissociations were

Author Manuscript Author Manuscript Author Manuscript Author Manuscript

encouraged by pipetting every 15 min. Cells were then washed with PBS plus 5% fetal calf serum (FCS) and passed through a 30 μm CellTrics filter (Sysmex). Cell suspensions were stained with 7-AAD (Sigma) and sorted on a MoFlo Astrios EQ cell sorter (Becman Coulter) at the Flow Cytometry Shared Resource Center (Duke University). Cells were collected in Buffer RLT Plus (Qiagen) and total RNA was prepared from each population using RNeasy Plus Micro Kit (QIAGEN). RNA samples were evaluated for concentration by Qubit (Thermo Fisher Scientific) and for integrity using an Agilent 2100 Bioanalyzer. Samples with an RNA integrity number (RIN) >7.0 were used for RNA sequencing (RNA-seq).

Clontech Ultra low libraries were prepared in triplicate and sequenced using the Illumina HiSeq 2000 50 bp single-end read platform. Sequencing data were uploaded to the Galaxy Web platform, and we used the public server at https://usegalaxy.org for analysis (Afgan et al., 2018). Reads were mapped to the GRCz10 (danRer10) zebrafish genome using HISAT2 (Kim et al., 2015), and gene counts were analyzed using HTseq (Anders et al., 2015). HTseq-counts were input into DESeq2 (Love et al., 2014) to calculate differential expression for cell populations (Wopat et al., 2018). Genes were considered to be enriched in a population if their expression had a log2(fold change)³2 in comparison with the other population, with an adjusted p value of <0.05. Principal-component analysis was performed in R using the DESeq2 package. All KEGG pathway and GO term analysis was performed using DAVID Bioinformatics Resources 6.8 (Huang da et al., 2009a, b; Kanehisa and Goto, 2000). Heatmaps were generated using the gplots package in R.

Analysis of gene expression data—To process mouse ileum time course data (Figures S7A and S7B), normalized expression data from each replicate of time course data from GEO accession GSE8065 (Schjoldager et al., 2008) was clustered using LRE-enriched mouse orthologs. Data was gene median centered and hierarchically clustered using complete linkage with uncentered correlation by Cluster 3.0. GEO2R (https://www.ncbi.nlm.nih.gov/geo/geo2r/?acc=GSE8065) was used to generate $\log^2$ fold change data between day 32 and day 7 timepoints using all replicates with the default parameters. LRE-enriched mouse orthologs that were identified by clustering to be down regulated post-weaning were used as input for Enrichr 3.0 (https://amp.pharm.mssm.edu/Enrichr/). Lysosome genes were extracted from KEGG (https://www.genome.jp/dbget-bin/www_bget?pathway+mmu04142). Orthology definitions between zebrafish and mouse were downloaded from Ensembl BioMart Genes 96.

To compare the gene expression data of larval zebrafish intestine to that of adult zebrafish intestine (Wang et al., 2010) (Figure S7C), the Z-score values of the adult zebrafish segment 5 (ileum-like) relative to all remaining segments were median centered for each gene and the details of the data processing are described in (Lickwar et al., 2017).

RNA Isolation and Reverse Transcription PCR (RT-PCR)—RNA was extracted using the RNeasy Mini Kit (Qiagen) according to the manufacturer's protocol. cDNA was synthesized using First Strand cDNA Synthesis Kit (Roche). To generate cDNA for RT-PCR for *cubn*, Cubn_R primer, 5' GGCAGACATAACCAGTGGCT 3', was used for reverse transcription cDNA synthesis. To generate cDNA for RT-PCR for *amn* and *dab2*, poly dT

Author Manuscript Author Manuscript Author Manuscript Author Manuscript

primer was used for reverse transcription cDNA synthesis. Primers used for RT-PCR include: cubn_RT_F, 5’ CAGCAGTAACCCATGCCAGA 3’; cubn_RT_R, 5’ GGAACCCAGCGTGTTGAAAC 3’; dab2_RT_F, 5’ ACAGACGAGTTCCTCTTGGC 3’; dab2_RT_R, 5’ AGCCAAATGCCCGGTTATCA 3’; amn_RT_F, 5’ GGATGAGCTTGCCTGTGGAT 3’; amn_RT_R, 5’ GAATGAGGTGGCGTCTCGAA 3’; rpl13a_F, 5’ TCTGGAGGACTGTAAGAGGTATGC 3’; rpl13a_R, 5’ AGACGCACAATCTTGAGAGCAG 3’. *rpl13a* was used as standard for all RT-PCR experiments.

Quantitative PCR—Quantitative PCR was performed using a Bio-Rad CFX96 Real-Time System C1000 Thermocycler and SensiFAST™ SYBR No-ROX kit (Bioline). Reactions were performed in duplicate. Primers used include: rpl13a_F, TCTGGAGGACTGTAAGAGGTATGC; rpl13a_R, 5’ AGACGCACAATCTTGAGAGCAG 3’; ifabp_F, 5’ CCACTGTCAGGATCACACAAC 3’ ; ifabp_R, 5’ AGCCAGTTTCCTTTTCACCATG 3’; mtp_F, 5’ CGGATCGTCCTCTGCTTATTC 3’; mtp_R, 5’ GTTGTTGCTCTGACCGTAAATG 3’; lamp2_F, 5’ GTCTGCTCAGATAAACCATCCAC 3’; lamp2_R, 5’ TCATCATATCATCAGCATGAAC 3’; pllp_F, 5’ GTGGGTATTACCAGGGTCATC 3’; pllp_R, 5’ GGCTGTGTATAACAGGGTCTCC 3’. Expression levels were normalized to *rpl13a* for each cDNA set.

In Situ Hybridization—In situ probes for *lrp2a* and *cubn* were generated using the plasmids generously shared by Salim Abdelilah-Seyfried (Anzenberger et al., 2006). pGEMTeasy-lrp2a and pTOPO-cubilin plasmids were linearized using SpeI and BamHI, respectively, and subjected to *in vitro* transcription using T7 RNA polymerase (NEB) and T3 RNA polymerase (Roche), respectively. To make *in situ* probes for *dab2* and *amn*, *dab2* and *amn* were amplified from cDNA using the following primers: dab2_antisense probe_F, 5’ CCCAGTGGTCAAAAGTGCCT 3’; dab2_antisense probe_R, 5’ ATAGCTAATACGACTCACTATAGGGAGCTACTTCACTGTGCAGCT 3’; dab2_sense probe_F, 5’ ATAGCTAATACGACTCACTATAGGGGAAAGAAGAGCCCCCAGTGG 3’; dab2_sense probe_R, 5’ AGCTACTTCACTGTGCAGCT 3’; amn_antisense probe_F, 5’ GCTGCTGGGAGTGATTCCTT 3’; amn_antisense probe_R, 5’ ATAGCTAATACGACTCACTATAGGGTGAAGCTTGTGAGAACTTCCCA 3’; amn_sense probe_F, 5’ ATAGCTAATACGACTCACTATAGGGGCTGCTGGGAGTGATTCCTT 3’; amn_sense probe_R, 5’ TGAAGCTTGTGAGAACTTCCCA 3’. Using the T7 promoter sequence included in the reverse primers for antisense probes and in the forward primers for sense probes, the PCR products were subjected to *in vitro* transcription using T7 RNA Polymerase (NEB). All *in vitro* transcription reactions were performed with DIG RNA Labeling Mix (Roche) to make digoxygenin-labeled RNA. In situ hybridization for *lrp2a*, *cubn*, *dab2* and *amn* was performed as described previously (Navis et al., 2013). Briefly, 5–6 dpf EK embryos were fixed in 4% PFA, dehydrated in 100% MeOH, and rehydrated. Then samples were digested with Proteinase K, hybridized with in situ probes, washed multiple times, incubated with secondary antibody, and stained using BM-Purple (Roche). Images were acquired on a Discovery V20 stereoscope (Zeiss).

Author Manuscript Author Manuscript Author Manuscript Author Manuscript

Microscopy—Whole-mount confocal live imaging was performed on a Fluoview FV3000 (Olympus) confocal microscope equipped with 30×/1.05 silicone oil objective (Olympus) and Fluoview software (Olympus). Fish were mounted onto glass-bottom dishes in a 1.2% agarose mixture of egg water and 1× tricaine. Z-step size for z-stacks images was 1.5 μm. Digital stitching of confocal images (Figure 1D, 1I, 4D, S3A–D, S6A–D) was done in Fluoview software.

Electron Microscopy—Zebrafish larvae were fixed in 0.1M sodium cacodylate, and 2.5% glutaraldehyde (GA). Specimen preparation and staining was done as previously described (Garcia et al., 2017). Briefly, after fixation, samples were stained with osmium tetroxide and uranyl acetate. Then samples were then dehydrated in ethanol solutions of increasing concentration and embedded in resin blocks overnight and then embedded and cured in 60 degrees oven for 48 hr. Then thin sections were cut and post-stained with lead citrate and uranyl acetate and placed on copper grids for imaging.

Zebrafish growth and survival under controlled feeding conditions—For larval feeding experiments, 10 larvae/3L tank were placed on our recirculating Aquatic Habitats system at 6 dpf. For non-calorie restricted standard feeding condition, each tank was fed with larval AP100 (Zeigler; twice daily) and GM75 (Skretting; once daily) from 5 dpf to 12 dpf and with artemia (twice daily) and GM75 (once daily) from 13 dpf to 30 dpf. For calorie-restricted high-protein (HP) or low-protein (LP) diet feeding conditions, each tank was fed with 10 mg of HP or LP once a day. HP and LP custom diets were formulated to have 50.10% or 25.05% protein contents, respectively. Diets are formulated as described before (Smith et al., 2013a). Briefly, each diet was produced using chemically defined ingredients. Diets were mixed in an orbital mixer (Kitchen Aid), extruded with a Kitchen Aid extruder (KPEXTA) and were air-dried before storage. The detailed compositions of the diets are provided in the Table S1. The survival of fish was monitored up to 30 dpf. Then, surviving fish were collected and imaged at 30 dpf with an Axio Zoom.V16 Stereoscope (Zeiss) with ZEN pro 2012 software (Zeiss). Using the acquired images, fish standard lengths (Parichy et al., 2009) were measured with ImageJ. To acquire normalized body length of *cubn* and *dab2* mutants at 5 and 30 dpf (Figure 5D), the standard lengths of 5 dpf and 30 dpf *cubn* or *dab2* mutants were divided by the average standard length of the same age *cubn* or *dab2* heterozygous controls, respectively.

Immunofluorescence and Histology—Zebrafish larval and adult gut transverse 200 micron sections were cut with a vibratome (VT 1000S; Leica) and stained as described previously (Bagnat et al., 2007). In brief, larvae or adult gut were fixed in 4% PFA for 2 hours at room temperature or overnight at 4°C, washed in PBS, embedded in 5% low-melt agarose in PBS, sectioned with a vibratome and stained with an appropriate antibody. For immunofluorescence staining of mouse tissues, organs were embedded in OCT after perfusion with 4% PFA, frozen sections were collected using a Leica cryotome, and sections were stained as previously described (Sumigray et al., 2018). Briefly, sections were washed in PBS-T containing 0.2% Triton X-100, then incubated in blocking buffer (3% BSA, 5% NGS, 5% NDS in PBS-T) for 15 min. Sections were incubated in primary antibody diluted in blocking buffer for 15 min – 1 hr at room temperature. After washing in PBS-T, sections

Author Manuscript Author Manuscript Author Manuscript Author Manuscript

were incubated in secondary antibodies for 10 min, washed, then mounted for imaging. The following antibodies were used for immunohistochemistry: anti-Rab5 (GeneTex), anti-Rab7 (Cell Signaling), anti-Disabled-2/p96 (BD Bioscience), anti-LAMP2 (DSHB), anti-ATPase, (Na (+) K (+)) alpha subunit (DSHB), anti-β-catenin (Sigma). For histological analysis, mice were fixed by perfusion with 4 % PFA and then organs were harvested and fixed by immersion overnight. Tissues were then dehydrated in ethanol, infiltrated overnight, embedded in plastic resin the JB4-plus kit (Polysciences), and 1–2 micron sections were cut using a Reichert-jung UltraCut microtome equipped with a glass knife. Plastic sections were stained with Mayer's Hematoxylin, Eosin-Y, Periodic Acid-Schiff, or Oil Red O (Sigma), mounted with Cytoseal XYL, and imaged using either an Axioimager Z1 (Zeiss) or Axio Zoom.V16 Stereoscope (Zeiss).

***Ex vivo* mCherry uptake in mouse intestinal tissue—**For uptake experiments, Villin-CreER (el Marjou et al., 2004) Dab2 cKO were used. The mom was injected with 5 mg tamoxifen in corn oil (Sigma) on P0 and P3, and pups were sacrificed at P6. Loss of protein was confirmed by immunofluorescence staining. Proximal and distal small intestines were dissected from P6 neonatal mice and washed with HBSS. 150 μg of 20 mg/ml mCherry was injected into the lumen of a 2 cm segment of dissected intestine, and the intestine was cultured on a Transwell dish (Corning) containing L-WRN conditioned media for 1.5 hours at 37°C, flushed with HBSS and fixed in 4% PFA overnight. The intestines were then washed in PBS and embed in Optimal Cutting Temperature (TissueTek), and 8-mm sections were cut on a cryostat (Leica). Sections were allowed to dry, then fixed in 4% PFA for 8 min. Sections were then blocked in 5% Normal Goat Serum, 5% Normal Donkey Serum and 3% Bovine Serum Albumin in PBS + 0.2% Triton-X 100. Primary antibodies were incubated for 1 h at RT, followed by secondary antibodies for 10 min at RT. Slides were washed in PBS-T, then mounted in 90% glycerol in PBS plus 2.5 mg/ml *p*-Phenylenediamine (Sigma). Tissue sections were imaged on an AxioImager Z1 Microscope (Zeiss) with Apotome.2 attachment and 63X Plan-Apo 1.4 NA oil lens. Zen software (Zeiss) was used.

QUANTIFICATION AND STATISTICAL ANALYSIS

GraphPad Prism version 7.04. for Windows (GraphPad Software) and Microsoft Excel were used to analyze and plot data. Statistical analysis for the comparisons of larval survival rate (Figures 5A and 5B), larval body length measurement (Figures 5C and 6D) and mCherry accumulation in the pronephros (Figures S3C and S3D) was calculated from two-tailed unpaired *t*-tests in GraphPad Prism. Statistical analysis for *Dab2* WT and cKO mouse data including body length (Figure 7K), body weight (Figure 7L), average weight gain/day (Figure 7M) and duodenum diameter (Figure 7O) was calculated from two-tailed paired *t*-tests in GraphPad Prism. Information and measurements of individual *Dab2* WT and cKO mice are provided in the Table S2. Exact *p*-values, *t*-values and degree of freedom for all the *t*-tests are provided in the Table S3. Sample size for each experiment is indicated in the figure legend for each experiment.

Author Manuscript Author Manuscript Author Manuscript Author Manuscript

DATA AND CODE AVAILABITILY

Raw and processed data for the RNA-seq experiment (Figures 2A, 2B and S4) are available in GEO DataSets with the following accession number: GSE124970.

Supplementary Material

Refer to Web version on PubMed Central for supplementary material.

ACKNOWLEDGEMENTS

We thank Julie Underwood for mouse care, Ricardo Vancini for his help with electron microscopy, Alessandro De Simone for his help with quantitative analysis, the Duke Zebrafish Core for fish care, and the Duke Flow Cytometry Shared Resource for their help with FACS. We also thank Brian A. Link, Salim Abdelilah-Seyfried for zebrafish lines and reagents and Kalina Hristova for fluorescent protein plasmids. We would like to thank Ken Poss, Brigid Hogan and Chris Nicchitta for critical reading of the manuscript and members of the Bagnat lab for discussions. This work was supported by NIH grants 1R01-DK113123 and 1R01-DK121007 (to M.B), R01-DK117981 and R01-AR067203 (to T.L.), and R01DK081426 (to J.F.R.); NIH fellowship 1F31DK111137–01A1 and the Korea Kwanjeong Educational Foundation (J.P.), T32DK007568–26 (D.S.L.). M.B. is an HHMI Faculty Scholar.

REFERENCES

Afgan E, Baker D, Batut B, van den Beek M, Bouvier D, Cech M, Chilton J, Clements D, Coraor N, Grüning BA, et al. (2018). The Galaxy platform for accessible, reproducible and collaborative biomedical analyses: 2018 update. Nucleic Acids Res 46, W537–W544. [PubMed: 29790989]

Ahuja R, Yammani R, Bauer JA, Kalra S, Seetharam S, and Seetharam B (2008). Interactions of cubilin with megalin and the product of the amnionless gene (AMN): effect on its stability. Biochem J 410, 301–308. [PubMed: 17990981]

Alvers AL, Ryan S, Scherz PJ, Huisken J, and Bagnat M (2014). Single continuous lumen formation in the zebrafish gut is mediated by smoothened-dependent tissue remodeling. Development 141, 1110–1119. [PubMed: 24504339]

Amsellem S, Gburek J, Hamard G, Nielsen R, Willnow TE, Devuyst O, Nexo E, Verroust PJ, Christensen EI, and Kozyraki R (2010). Cubilin is essential for albumin reabsorption in the renal proximal tubule. J Am Soc Nephrol 21, 1859–1867. [PubMed: 20798259]

Anders S, Pyl PT, and Huber W (2015). HTSeq--a Python framework to work with high-throughput sequencing data. Bioinformatics 31, 166–169. [PubMed: 25260700]

André M, Ando S, Ballagny C, Durliat M, Poupard G, Briançon C, and Babin PJ (2000). Intestinal fatty acid binding protein gene expression reveals the cephalocaudal patterning during zebrafish gut morphogenesis. Int J Dev Biol 44, 249–252. [PubMed: 10794084]

Anzenberger U, Bit-Avragim N, Rohr S, Rudolph F, Dehmel B, Willnow TE, and Abdelilah-Seyfried S (2006). Elucidation of megalin/LRP2-dependent endocytic transport processes in the larval zebrafish pronephros. J Cell Sci 119, 2127–2137. [PubMed: 16638803]

Asari M, Kawaguchi N, Wakui S, Fukaya K, and Kano Y (1987). Development of the bovine ileal mucosa. Acta Anat (Basel) 129, 315–324. [PubMed: 3630620]

Bagnat M, Cheung ID, Mostov KE, and Stainier DY (2007). Genetic control of single lumen formation in the zebrafish gut. Nat Cell Biol 9, 954–960. [PubMed: 17632505]

Bates JM, Mittge E, Kuhlman J, Baden KN, Cheesman SE, and Guillemin K (2006). Distinct signals from the microbiota promote different aspects of zebrafish gut differentiation. Dev Biol 297, 374–386. [PubMed: 16781702]

Buchanan RM, Tetland S, and Wilson HL (2012). Low dose antigen exposure for a finite period in newborn rats prevents induction of mucosal tolerance. PLoS One 7, e51437. [PubMed: 23251533]

Carten JD, Bradford MK, and Farber SA (2011). Visualizing digestive organ morphology and function using differential fatty acid metabolism in live zebrafish. Dev Biol 360, 276–285. [PubMed: 21968100]

Author Manuscript Author Manuscript Author Manuscript Author Manuscript

Christensen EI, and Nielsen R (2007). Role of megalin and cubilin in renal physiology and pathophysiology. Rev Physiol Biochem Pharmacol 158, 1–22. [PubMed: 17729440]

Cocchiaro JL, and Rawls JF (2013). Microgavage of zebrafish larvae. J Vis Exp, e4434. [PubMed: 23463135]

Coulthard MG (2015). Oedema in kwashiorkor is caused by hypoalbuminaemia. Paediatr Int Child H 35, 83–89.

el Marjou F, Janssen KP, Chang BH, Li M, Hindie V, Chan L, Louvard D, Chambon P, Metzger D, and Robine S (2004). Tissue-specific and inducible Cre-mediated recombination in the gut epithelium. Genesis 39, 186–193. [PubMed: 15282745]

Ellis K, Bagwell J, and Bagnat M (2013). Notochord vacuoles are lysosome-related organelles that function in axis and spine morphogenesis. J Cell Biol 200, 667–679. [PubMed: 23460678]

Fyfe JC, Madsen M, Hojrup P, Christensen EI, Tanner SM, de la Chapelle A, He Q, and Moestrup SK (2004). The functional cobalamin (vitamin B12)-intrinsic factor receptor is a novel complex of cubilin and amnionless. Blood 103, 1573–1579. [PubMed: 14576052]

Garcia J, Bagwell J, Njaine B, Norman J, Levic DS, Wopat S, Miller SE, Liu X, Locasale JW, Stainier DYR, et al. (2017). Sheath Cell Invasion and Trans-differentiation Repair Mechanical Damage Caused by Loss of Caveolae in the Zebrafish Notochord. Curr Biol 27, 1982–1989.e1983. [PubMed: 28648824]

Golden MH (1998). Oedematous malnutrition. Br Med Bull 54, 433–444. [PubMed: 9830208]

Gonnella PA, and Neutra MR (1984). Membrane-bound and fluid-phase macromolecules enter separate prelysosomal compartments in absorptive cells of suckling rat ileum. J Cell Biol 99, 909–917. [PubMed: 6470044]

Graney DO (1968). The uptake of ferritin by ileal absorptive cells in suckling rats. An electron microscope study. Am J Anat 123, 227–254. [PubMed: 5701162]

Harper J, Mould A, Andrews RM, Bikoff EK, and Robertson EJ (2011). The transcriptional repressor Blimp1/Prdm1 regulates postnatal reprogramming of intestinal enterocytes. Proc Natl Acad Sci U S A 108, 10585–10590. [PubMed: 21670299]

He Q, Madsen M, Kilkenney A, Gregory B, Christensen EI, Vorum H, Hojrup P, Schaffer AA, Kirkness EF, Tanner SM, et al. (2005). Amnionless function is required for cubilin brush-border expression and intrinsic factor-cobalamin (vitamin B12) absorption in vivo. Blood 106, 1447–1453. [PubMed: 15845892]

Henning SJ (1985). Ontogeny of enzymes in the small intestine. Annu Rev Physiol 47, 231–245. [PubMed: 3888075]

Her GM, Chiang CC, and Wu JL (2004). Zebrafish intestinal fatty acid binding protein (I-FABP) gene promoter drives gut-specific expression in stable transgenic fish. Genesis 38, 26–31. [PubMed: 14755801]

Hill JH, Franzosa EA, Huttenhower C, and Guillemin K (2016). A conserved bacterial protein induces pancreatic beta cell expansion during zebrafish development. Elife 5.

Huang da W, Sherman BT, and Lempicki RA (2009a). Bioinformatics enrichment tools: paths toward the comprehensive functional analysis of large gene lists. Nucleic Acids Res 37, 1–13. [PubMed: 19033363]

Huang da W, Sherman BT, and Lempicki RA (2009b). Systematic and integrative analysis of large gene lists using DAVID bioinformatics resources. Nat Protoc 4, 44–57. [PubMed: 19131956]

Johannes L, Parton RG, Bassereau P, and Mayor S (2015). Building endocytic pits without clathrin. Nat Rev Mol Cell Biol 16, 311–321. [PubMed: 25857812]

Kanehisa M, and Goto S (2000). KEGG: kyoto encyclopedia of genes and genomes. Nucleic Acids Res 28, 27–30. [PubMed: 10592173]

Kim D, Langmead B, and Salzberg SL (2015). HISAT: a fast spliced aligner with low memory requirements. Nat Methods 12, 357–360. [PubMed: 25751142]

Kleinman RE, and Walker WA (1984). Antigen processing and uptake from the intestinal tract. Clin Rev Allergy 2, 25–37. [PubMed: 6370411]

Kozyraki R, and Gofflot F (2007). Multiligand endocytosis and congenital defects: roles of cubilin, megalin and amnionless. Curr Pharm Des 13, 3038–3046. [PubMed: 17979745]

Author Manuscript Author Manuscript Author Manuscript Author Manuscript

Kraehenbuhl JP, and Campiche MA (1969). Early stages of intestinal absorption of specific antibiodies in the newborn. An ultrastructural, cytochemical, and immunological study in the pig, rat, and rabbit. J Cell Biol 42, 345–365. [PubMed: 5815502]

Kulkarni DH, and Newberry RD (2019). Intestinal Macromolecular Transport Supporting Adaptive Immunity. Cell Mol Gastroenterol Hepatol.

Kwan KM, Fujimoto E, Grabher C, Mangum BD, Hardy ME, Campbell DS, Parant JM, Yost HJ, Kanki JP, and Chien CB (2007). The Tol2kit: a multisite gateway-based construction kit for Tol2 transposon transgenesis constructs. Dev Dyn 236, 3088–3099. [PubMed: 17937395]

Larsen C, Etzerodt A, Madsen M, Skjodt K, Moestrup SK, and Andersen CBF (2018). Structural assembly of the megadalton-sized receptor for intestinal vitamin B12 uptake and kidney protein reabsorption. Nat Commun 9, 5204. [PubMed: 30523278]

Lauffer BE, Melero C, Temkin P, Lei C, Hong W, Kortemme T, and von Zastrow M (2010). SNX27 mediates PDZ-directed sorting from endosomes to the plasma membrane. J Cell Biol 190, 565–574. [PubMed: 20733053]

Lawe DC, Patki V, Heller-Harrison R, Lambright D, and Corvera S (2000). The FYVE domain of early endosome antigen 1 is required for both phosphatidylinositol 3-phosphate and Rab5 binding. Critical role of this dual interaction for endosomal localization. J Biol Chem 275, 3699–3705. [PubMed: 10652369]

Lickwar CR, Camp JG, Weiser M, Cocchiaro JL, Kingsley DM, Furey TS, Sheikh SZ, and Rawls JF (2017). Genomic dissection of conserved transcriptional regulation in intestinal epithelial cells. PLoS Biol 15, e2002054. [PubMed: 28850571]

Love MI, Huber W, and Anders S (2014). Moderated estimation of fold change and dispersion for RNA-seq data with DESeq2. Genome Biol 15, 550. [PubMed: 25516281]

Madison BB, Dunbar L, Qiao XT, Braunstein K, Braunstein E, and Gumucio DL (2002). Cis elements of the villin gene control expression in restricted domains of the vertical (crypt) and horizontal (duodenum, cecum) axes of the intestine. J Biol Chem 277, 33275–33283. [PubMed: 12065599]

Marjoram L, Alvers A, Deerhake ME, Bagwell J, Mankiewicz J, Cocchiaro JL, Beerman RW, Willer J, Sumigray KD, Katsanis N, et al. (2015). Epigenetic control of intestinal barrier function and inflammation in zebrafish. Proc Natl Acad Sci U S A 112, 2770–2775. [PubMed: 25730872]

Marza E, Barthe C, André M, Villeneuve L, Hélou C, and Babin PJ (2005). Developmental expression and nutritional regulation of a zebrafish gene homologous to mammalian microsomal triglyceride transfer protein large subunit. Dev Dyn 232, 506–518. [PubMed: 15614773]

Maurer ME, and Cooper JA (2005). Endocytosis of megalin by visceral endoderm cells requires the Dab2 adaptor protein. J Cell Sci 118, 5345–5355. [PubMed: 16263760]

Mishra SK, Keyel PA, Hawryluk MJ, Agostinelli NR, Watkins SC, and Traub LM (2002). Disabled-2 exhibits the properties of a cargo-selective endocytic clathrin adaptor. EMBO J 21, 4915–4926. [PubMed: 12234931]

Moreno-Mateos MA, Vejnar CE, Beaudoin JD, Fernandez JP, Mis EK, Khokha MK, and Giraldez AJ (2015). CRISPRscan: designing highly efficient sgRNAs for CRISPR-Cas9 targeting in vivo. Nat Methods 12, 982–988. [PubMed: 26322839]

Morris SM, Tallquist MD, Rock CO, and Cooper JA (2002). Dual roles for the Dab2 adaptor protein in embryonic development and kidney transport. EMBO J 21, 1555–1564. [PubMed: 11927540]

Muncan V, Heijmans J, Krasinski SD, Buller NV, Wildenberg ME, Meisner S, Radonjic M, Stapleton KA, Lamers WH, Biemond I, et al. (2011). Blimp1 regulates the transition of neonatal to adult intestinal epithelium. Nat Commun 2, 452. [PubMed: 21878906]

Murdoch CC, Espenschied ST, Matty MA, Mueller O, Tobin DM, and Rawls JF (2019). Intestinal Serum amyloid A suppresses systemic neutrophil activation and bactericidal activity in esponse to microbiota colonization. PLoS Pathog 15, e1007381. [PubMed: 30845179]

Navis A, Marjoram L, and Bagnat M (2013). Cftr controls lumen expansion and function of Kupffer's vesicle in zebrafish. Development 140, 1703–1712. [PubMed: 23487313]

Neff MM, Neff JD, Chory J, and Pepper AE (1998). dCAPS, a simple technique for the genetic analysis of single nucleotide polymorphisms: experimental applications in Arabidopsis thaliana genetics. Plant J 14, 387–392. [PubMed: 9628033]

Author Manuscript Author Manuscript Author Manuscript Author Manuscript

Ng AN, de Jong-Curtain TA, Mawdsley DJ, White SJ, Shin J, Appel B, Dong PD, Stainier DY, and Heath JK (2005). Formation of the digestive system in zebrafish: III. Intestinal epithelium morphogenesis. Dev Biol 286, 114–135. [PubMed: 16125164]

Nielsen R, Christensen EI, and Birn H (2016). Megalin and cubilin in proximal tubule protein reabsorption: from experimental models to human disease. Kidney Int 89, 58–67. [PubMed: 26759048]

Parichy DM, Elizondo MR, Mills MG, Gordon TN, and Engeszer RE (2009). Normal table of postembryonic zebrafish development: staging by externally visible anatomy of the living fish. Dev Dyn 238, 2975–3015. [PubMed: 19891001]

Rawls JF, Samuel BS, and Gordon JI (2004). Gnotobiotic zebrafish reveal evolutionarily conserved responses to the gut microbiota. Proc Natl Acad Sci U S A 101, 4596–4601. [PubMed: 15070763]

Rebsamen M, Pochini L, Stasyk T, de Araujo ME, Galluccio M, Kandasamy RK, Snijder B, Fauster A, Rudashevskaya EL, Bruckner M, et al. (2015). SLC38A9 is a component of the lysosomal amino acid sensing machinery that controls mTORC1. Nature 519, 477–481. [PubMed: 25561175]

Reinhardt MC (1984). Macromolecular absorption of food antigens in health and disease. Ann Allergy 53, 597–601. [PubMed: 6439076]

Rink J, Ghigo E, Kalaidzidis Y, and Zerial M (2005). Rab conversion as a mechanism of progression from early to late endosomes. Cell 122, 735–749. [PubMed: 16143105]

Robberecht P, Deschodt-Lanckman M, Camus J, Bruylands J, and Christophe J (1971). Rat pancreatic hydrolases from birth to weaning and dietary adaptation after weaning. Am J Physiol 221, 376–381. [PubMed: 5555811]

Rodriguez-Fraticelli AE, Bagwell J, Bosch-Fortea M, Boncompain G, Reglero-Real N, Garcia-Leon MJ, Andres G, Toribio ML, Alonso MA, Millan J, et al. (2015). Developmental regulation of apical endocytosis controls epithelial patterning in vertebrate tubular organs. Nat Cell Biol 17, 241–250. [PubMed: 25706235]

Rombout JH, Lamers CH, Helfrich MH, Dekker A, and Taverne-Thiele JJ (1985). Uptake and transport of intact macromolecules in the intestinal epithelium of carp (Cyprinus carpio L.) and the possible immunological implications. Cell Tissue Res 239, 519–530. [PubMed: 3986879]

Sarabipour S, King C, and Hristova K (2014). Uninduced high-yield bacterial expression of fluorescent proteins. Anal Biochem 449, 155–157. [PubMed: 24378720]

Schjoldager KT, Maltesen HR, Balmer S, Lund LR, Claesson MH, Sjostrom H, Troelsen JT, and Olsen J (2008). Cellular cross talk in the small intestinal mucosa: postnatal lymphocytic immigration elicits a specific epithelial transcriptional response. Am J Physiol Gastrointest Liver Physiol 294, G1335–1343. [PubMed: 18388184]

Semova I, Carten JD, Stombaugh J, Mackey LC, Knight R, Farber SA, and Rawls JF (2012). Microbiota regulate intestinal absorption and metabolism of fatty acids in the zebrafish. Cell Host Microbe 12, 277–288. [PubMed: 22980325]

Shaner NC, Campbell RE, Steinbach PA, Giepmans BN, Palmer AE, and Tsien RY (2004). Improved monomeric red, orange and yellow fluorescent proteins derived from Discosoma sp. red fluorescent protein. Nat Biotechnol 22, 1567–1572. [PubMed: 15558047]

Shinoda H, Shannon M, and Nagai T (2018). Fluorescent Proteins for Investigating Biological Events in Acidic Environments. Int J Mol Sci 19.

Smith DL Jr., Barry RJ, Powell ML, Nagy TR, D'Abramo LR, and Watts SA (2013a). Dietary protein source influence on body size and composition in growing zebrafish. Zebrafish 10, 439–446. [PubMed: 23656299]

Smith MI, Yatsunenko T, Manary MJ, Trehan I, Mkakosya R, Cheng J, Kau AL, Rich SS, Concannon P, Mychaleckyj JC, et al. (2013b). Gut microbiomes of Malawian twin pairs discordant for kwashiorkor. Science 339, 548–554. [PubMed: 23363771]

Strope S, Rivi R, Metzger T, Manova K, and Lacy E (2004). Mouse amnionless, which is required for primitive streak assembly, mediates cell-surface localization and endocytic function of cubilin on visceral endoderm and kidney proximal tubules. Development 131, 4787–4795. [PubMed: 15342463]

Author Manuscript Author Manuscript Author Manuscript Author Manuscript

Subedi A, Macurak M, Gee ST, Monge E, Goll MG, Potter CJ, Parsons MJ, and Halpern ME (2014). Adoption of the Q transcriptional regulatory system for zebrafish transgenesis. Methods 66, 433–440. [PubMed: 23792917]

Sumigray KD, Terwilliger M, and Lechler T (2018). Morphogenesis and compartmentalization of the intestinal crypt. Dev Cell 45, 183–197.e185. [PubMed: 29689194]

Swanson JA, Yirinec BD, and Silverstein SC (1985). Phorbol esters and horseradish peroxidase stimulate pinocytosis and redirect the flow of pinocytosed fluid in macrophages. J Cell Biol 100, 851–859. [PubMed: 3972898]

Trahair JF, and Robinson PM (1989). Enterocyte ultrastructure and uptake of immunoglobulins in the small intestine of the neonatal lamb. J Anat 166, 103–111. [PubMed: 2621130]

Turfkruyer M, Rekima A, Macchiaverni P, Le Bourhis L, Muncan V, van den Brink GR, Tulic MK, and Verhasselt V (2016). Oral tolerance is inefficient in neonatal mice due to a physiological vitamin A deficiency. Mucosal Immunol 9, 479–491. [PubMed: 26530133]

Vazquez-Carretero MD, Palomo M, Garcia-Miranda P, Sanchez-Aguayo I, Peral MJ, Calonge ML, and Ilundain AA (2014). Dab2, megalin, cubilin and amnionless receptor complex might mediate intestinal endocytosis in the suckling rat. J Cell Biochem 115, 510–522. [PubMed: 24122887]

Veth KN, Willer JR, Collery RF, Gray MP, Willer GB, Wagner DS, Mullins MC, Udvadia AJ, Smith RS, John SW, et al. (2011). Mutations in zebrafish lrp2 result in adult-onset ocular pathogenesis that models myopia and other risk factors for glaucoma. PLoS Genet 7, e1001310. [PubMed: 21379331]

Wallace KN, Akhter S, Smith EM, Lorent K, and Pack M (2005). Intestinal growth and differentiation in zebrafish. Mech Dev 122, 157–173. [PubMed: 15652704]

Wang Z, Du J, Lam SH, Mathavan S, Matsudaira P, and Gong Z (2010). Morphological and molecular evidence for functional organization along the rostrocaudal axis of the adult zebrafish intestine. BMC Genomics 11, 392. [PubMed: 20565988]

Westerfield M (2000). The Zebrafish Book. A Guide for The Laboratory Use of Zebrafish (Danio rerio), Vol 385.

Williams CD, Oxon BM, and Lond H (2003). Kwashiorkor: a nutritional disease of children associated with a maize diet. 1935. Bull World Health Organ 81, 912–913. [PubMed: 14997245]

Wilson JM, Whitney JA, and Neutra MR (1991). Biogenesis of the apical endosome-lysosome complex during differentiation of absorptive epithelial cells in rat ileum. J Cell Sci 100 (Pt 1), 133–143. [PubMed: 1795021]

Wopat S, Bagwell J, Sumigray KD, Dickson AL, Huitema LFA, Poss KD, Schulte-Merker S, and Bagnat M (2018). Spine patterning is guided by segmentation of the notochord sheath. Cell Rep 22, 2026–2038. [PubMed: 29466731]

Yin L, Jao L-E, and Chen W (2015). Generation of targeted mutations in zebrafish using the crispr/cas system. Methods Mol Biol 1332, 205–217. [PubMed: 26285757]

Zabielski R, Godlewski MM, and Guilloteau P (2008). Control of development of gastrointestinal system in neonates. J Physiol Pharmacol 59 Suppl 1, 35–54.

Zhang FX, Chen JP, Yang F, and Li LQ (2005). Effects of age and suckling on chymosin and pepsin activities in abomasums of goat kids. Int J Dairy Technol 58, 115–118.

Zohn IE, and Sarkar AA (2010). The visceral yolk sac endoderm provides for absorption of nutrients to the embryo during neurulation. Birth Defects Res A Clin Mol Teratol 88, 593–600. [PubMed: 20672346]

Author Manuscript Author Manuscript Author Manuscript Author Manuscript

HIGHLIGHTS

- Lysosome Rich Enterocytes internalize and digest dietary protein intracellularly
- LREs are conserved between zebrafish and mammals
- Cubn, Amn and Dab2 mediate high capacity protein uptake in LREs
- Loss of LRE function impairs growth and survival in zebrafish and mice

Author Manuscript
Author Manuscript
Author Manuscript
Author Manuscript

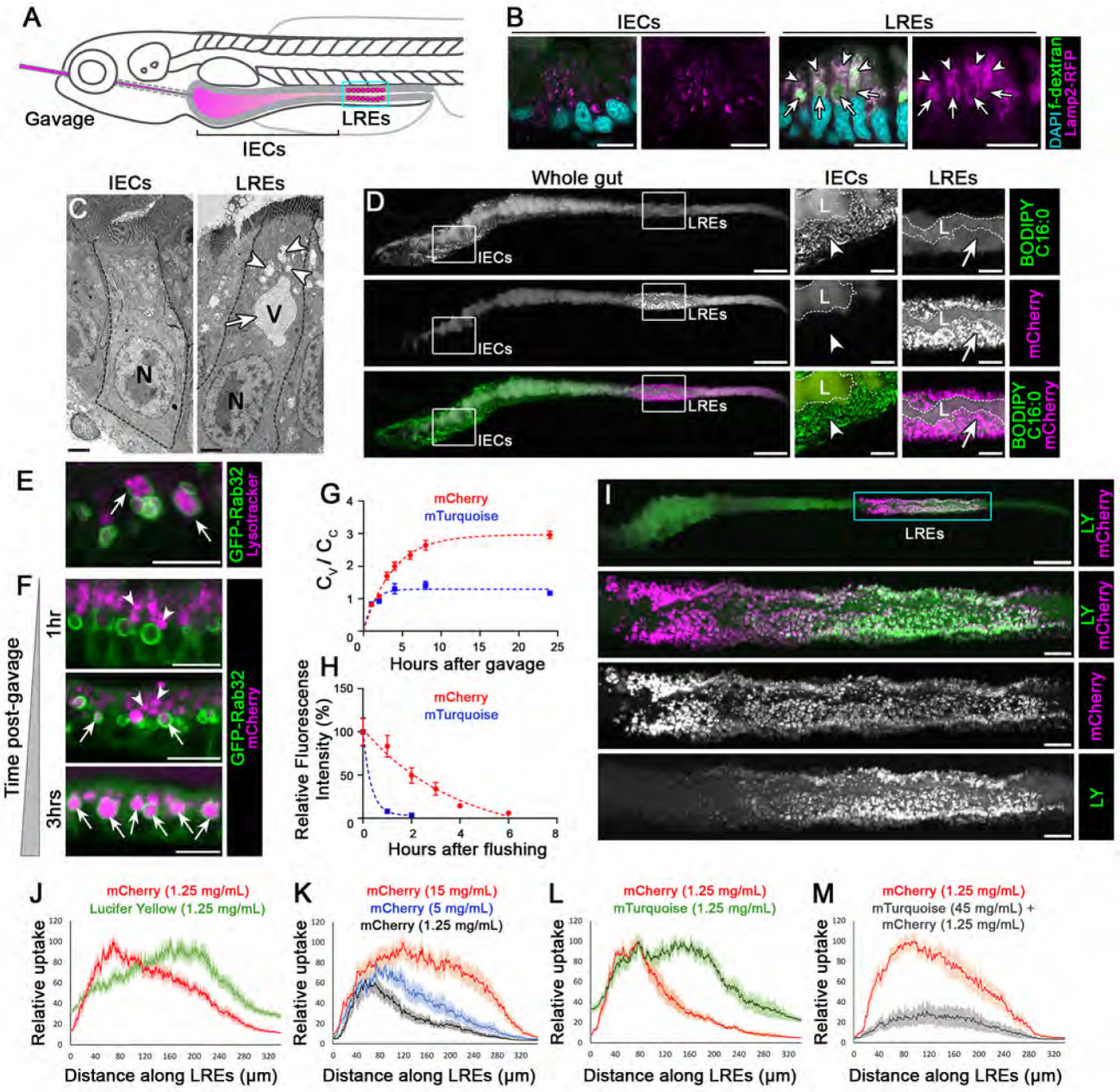

Figure 1. Luminal proteins are internalized and digested intracellularly by LREs in the zebrafish intestine.

(A) Cartoon depicting gavage approach for studying luminal cargo uptake into LREs (cyan box) in the larval zebrafish intestine. **(B)** Confocal images of cross sections of intestinal segments showing IECs and LREs from a 6 dpf larva following gavage with fluorescent dextran (fDex). Lamp2 is highly expressed in LREs and localizes to endosomes (arrowheads) and lysosomal vacuoles (arrows) that accumulate internalized fDex. n≥ 10 animals. Scale bars=10 μm. **(C)** EM images of an IEC and an LRE. Arrowheads mark endosomes and an arrow the lysosomal vacuole. N=nucleus; V= vacuole. n≥ 5 animals. Scale bars=2 μm. **(D)** Live confocal images of a 6 dpf larval zebrafish intestine following gavage and internalization of BODIPY C16:0 and mCherry. IECs take lipids and LREs

Author Manuscript Author Manuscript Author Manuscript Author Manuscript

protein. L=lumen. Insets show magnified images marking lipid droplets (arrowheads) in IECs and lysosomal vacuoles in LREs (arrows). n=5. Scale bars=100 μm (whole gut images), 25 μm (magnified images). **(E)** Live confocal images of LREs of 6 dpf larva expressing GFP-Rab32a 1 hr after gavage with lysotracker, which labels vacuoles (arrows). n≥ 10 animals. Scale bar=10 μm. **(F)** Live confocal images of LREs of 6 dpf larvae expressing GFP-Rab32a that were gavaged with mCherry. Luminal protein (mCherry) was internalized, migrated through apical endosomes (arrowheads), and progressively accumulated in LRE vacuoles (arrows). Scale bars= 10 μm. **(G)** Quantitation of mCherry and mTurquoise accumulation in LRE vacuoles (Cv) respect to total cellular mean pixel intensity (Cc) over time after gavaging with 1.25 mg/ml of mCherry or mTurquoise. Data are fitted with the model Cv/Cc = k_in/k_ex *(1-exp(−k_ex*X)) where k_in is the vacuole internalization rate and k_ex is the degradation rate. n≥28; LREs from at least 6 animals per timepoint. **(H)** Quantitation of mCherry and mTurquoise degradation in LREs over time following gavage with 1.25 mg/ml mCherry or 5 mg/ml mTurquoise for an hour. Data are fitted with one phase decay model (dotted lines). n≥ 9 animals per timepoint. **(I)** Live confocal image of a 6 dpf larva gavaged with Lucifer Yellow (LY) and mCherry. Cyan box indicates magnified inset of LREs in lower panels. Scale bar=100 μm (whole gut image), 20 μm (magnified images). **(J)** Internalization profiles of LY and mCherry along LREs (n=12). **(K)** Internalization profiles along LRE region following gavage with increasing concentrations of mCherry: 1.25 mg/ml (n=7), 5 mg/ml (n=8), 15 mg/ml (n=9). **(L)** Internalization profiles along LRE region of mCherry and mTurquoise (n=8). **(M)** Internalization profiles along LRE region of mCherry following gavage with either mCherry alone (n=7) or both mCherry + excess mTurquoise to outcompete mCherry uptake (n=7). Data are means ± S.E.M. in panels G, H, J-M. Whole gut images in panels D and I are digitally stitched. See also Figure S1, S2 and S3.

Author Manuscript Author Manuscript Author Manuscript Author Manuscript

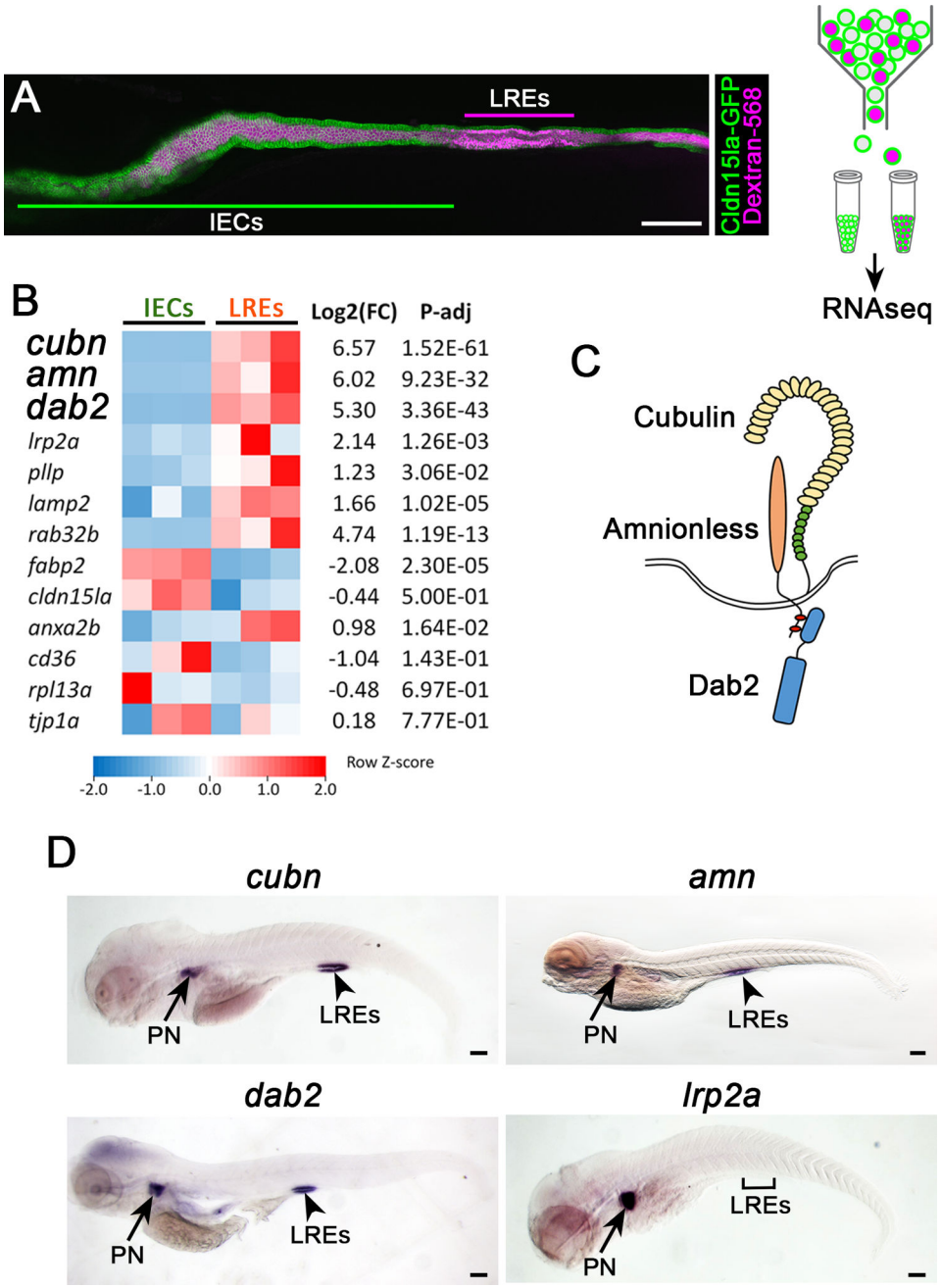

Figure 2. LREs specifically express a multiligand endocytic machinery composed of Cubn, Amn and Dab2.

(A) Isolation and analysis of gene expression profiles in LREs versus IEC. 6 dpf larvae expressing Cldn15la-GFP throughout the gut were gavaged with alexa-568 dextran (left panel) and subjected to FACS to isolate IECs and LREs for RNAseq (right panel). Scale bar=100 μm. **(B)** Heatmap of RNAseq data depicting expression levels of selected genes in LREs and IECs. Three independent samples for each cell population were used for RNAseq experiment. **(C)** Cartoon illustrating the multiligand endocytic machinery composed of Cubn, Amn and Dab2. **(D)** In situ hybridization of *cubn* (cubilin), *amn* (amnionless), *dab2*,

Author Manuscript Author Manuscript Author Manuscript Author Manuscript

and *lrp2a (*megalin)*. cubn, amn*, and *dab2* transcripts are enriched in LREs and pronephros. Bracket marks LRE region devoid of *lrp2a* transcript expression. PN=pronephros. n≥ 20 animals. See also Figure S4 and S5.

Author Manuscript Author Manuscript Author Manuscript Author Manuscript

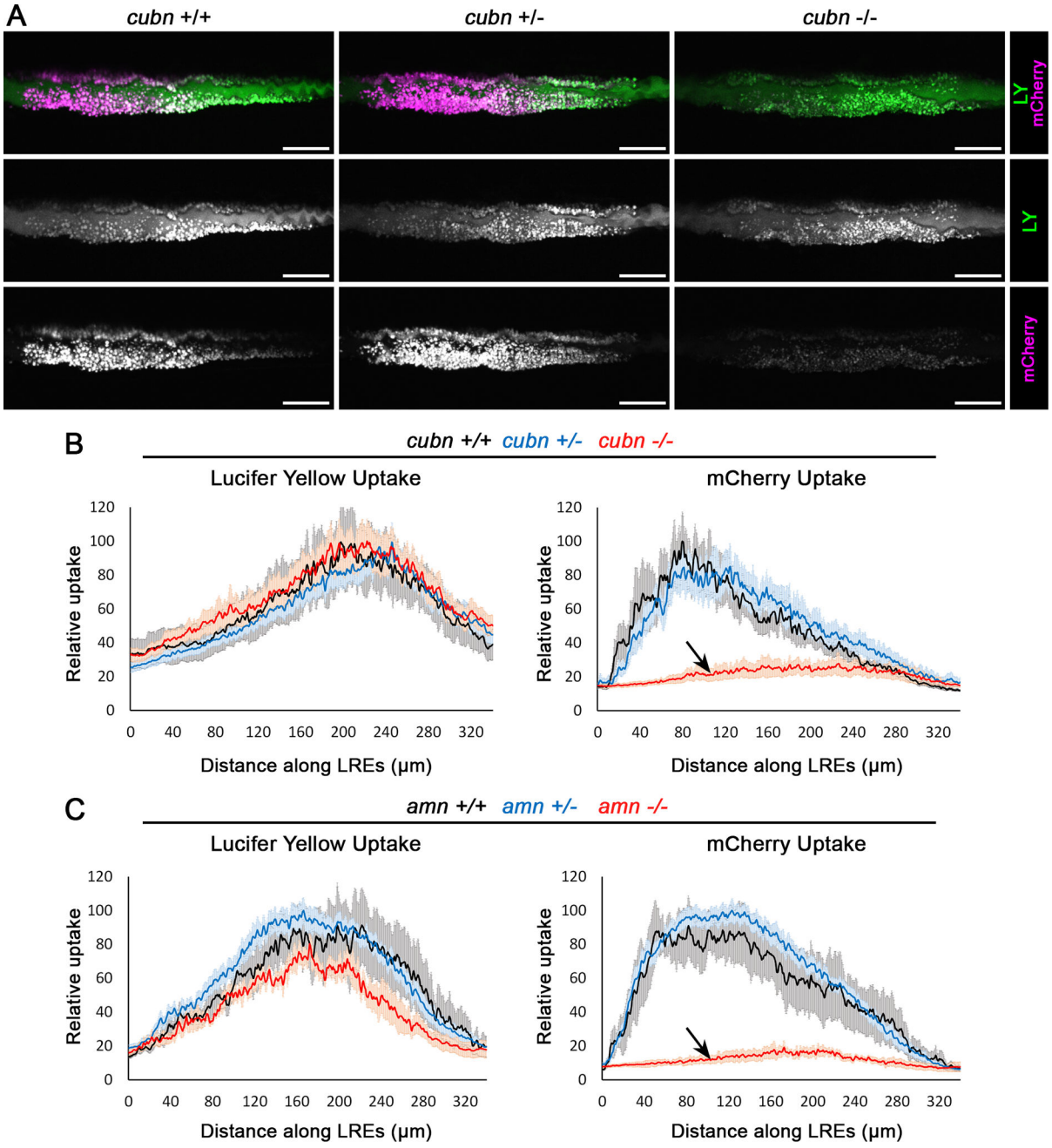

Figure 3. The Cubn/Amn endocytic receptor complex mediates protein uptake in LREs.

(A) Live confocal images showing LY and mCherry uptake in LREs of *cubn*^{pd1169} *+/+, +/−, −/−* 6 dpf larvae. Larvae were imaged 5 hours after gavage. *cubn* ^{pd1169} mutants show selective loss of protein (mCherry) internalization. Scale bar=50 μm. **(B, C)** Internalization profiles of LY (Left) and mCherry (Right) of protein uptake (arrows). Data are means ± S.E.M. See also Figure S5 and S6.

Author Manuscript Author Manuscript Author Manuscript Author Manuscript

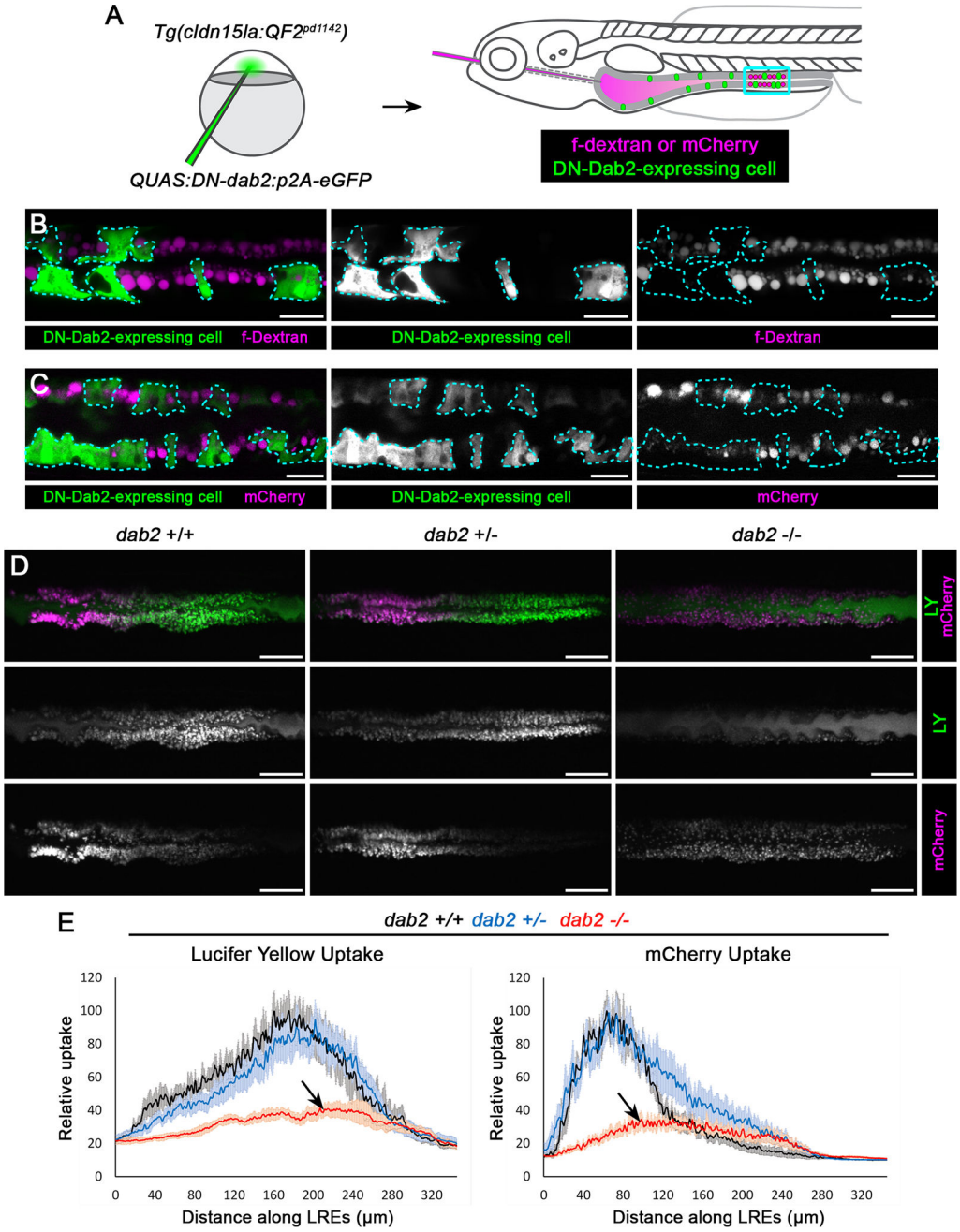

Figure 4. Dab2 mediates fluid-phase and receptor-dependent endocytosis in LREs.

(A) Experimental scheme to mosaically inhibit Dab2 function. A dominant-negative (DN), *QUAS:DN-Dab2:p2A-EGFP*, construct was injected into *Tg(cldn15la:QF2^{pd1142})* embryos to co-express DN-Dab2 and soluble eGFP to mark expressing cells in IECs and LREs. Larvae mosaically expressing DN-Dab2 were then gavaged with fDex or mCherry and imaged 5 hours post-gavage. **(B, C)** Live confocal images of fDex or mCherry uptake in 6 dpf *Tg(cldn15la:QF2 ^{pd1142})* LREs mosaically expressing DN-Dab2. LREs expressing DN-Dab2 (marked with dotted line) showed reduced fDex (n=6) (B) and mCherry (n=3) (C) uptake relative to WT neighboring LREs. Scale bar=20 μm. **(D)** Live confocal images of 6

Author Manuscript Author Manuscript Author Manuscript Author Manuscript

dpf *dab2*^{pd1162} +/+, +/−, −/− LREs imaged 5 hours after gavage with LY and mCherry. Scale bar=50 μm. **(E)** Internalization profiles of LY (Left) and mCherry (Right) from 6 dpf *dab2*^{pd1162} *+/+* (n=5), *+/−* (n=8), *−/−* (n=6) larvae. *dab2* mutants showed impaired internalization of both protein (mCherry) and fluid-phase (LY) cargos (arrows). Data are means ± S.E.M. Images in panel C are digitally stitched. See also Figure S5 and S6.

Author Manuscript Author Manuscript Author Manuscript Author Manuscript

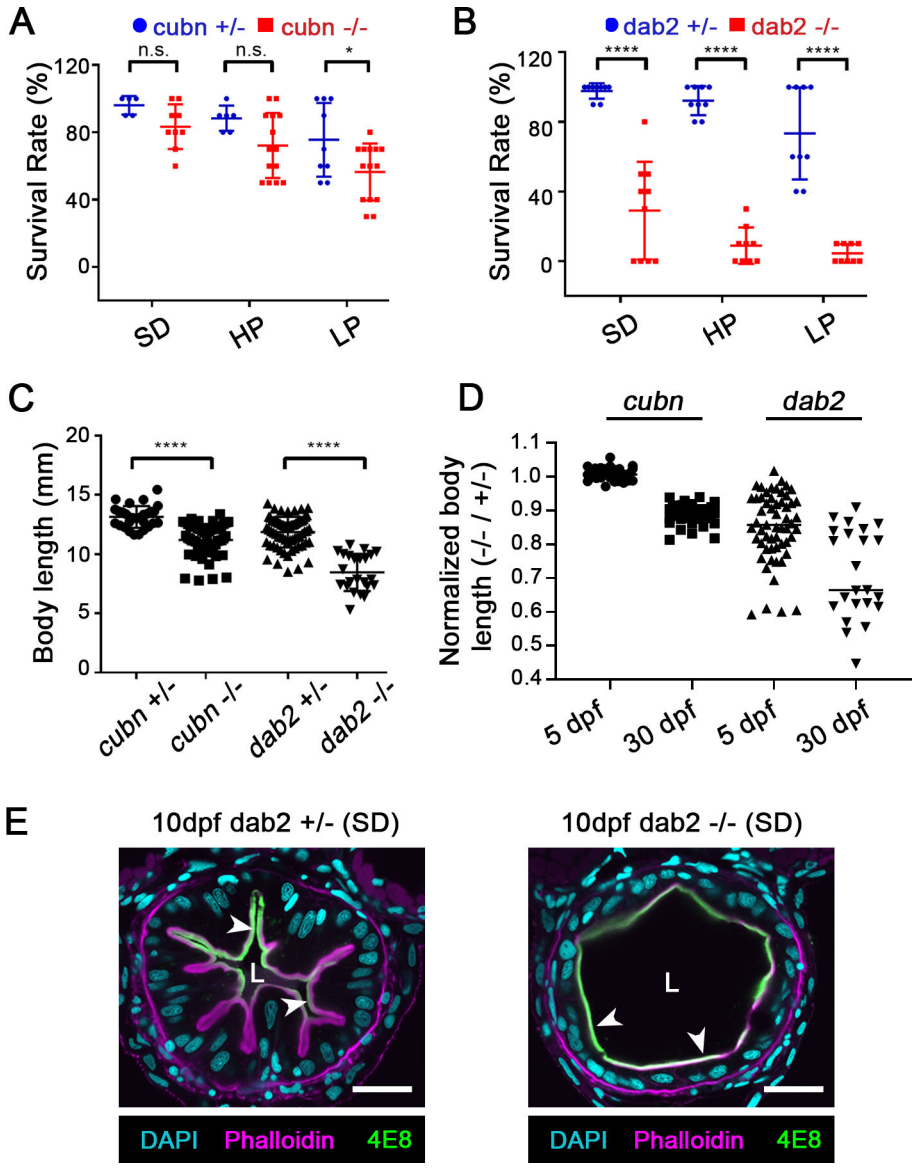

Figure 5. Loss of LRE protein uptake impairs growth and survival in larval zebrafish.

(A, B) Survival rates of *cubn* ^{pd1169} +/−, −/− (A), and *dab2* ^{pd1162} *+/−, −/−* (B) 30 dpf larvae raised under different feeding conditions: non-calorie restricted standard diet (SD), calorie-restricted high-protein diet (HP) and calorie-restricted low-protein diet (LP). n=5, 9, 6, 14, 9, 14 (A; left to right), n=9, 10, 9, 9, 9, 9 (B; left to right). Data points are the survival rates of each tank subjected to the experiment. **(C)** Comparison of body lengths of *cubn* ^{pd1169} +/− (n=29*)*, −/− *(*n=57*)*, and *dab2* ^{pd1162} *+/−* (n=69*)*, *−/−* (n=23*)* 30 dpf larvae raised under a non-calorie restricted SD. Data points are the body lengths of individual 30 dpf larvae that survived until the end of the feeding experiments. **(D)** Quantitation of mutant/heterozygous control body length ratios for *cubn* ^{pd1169} and *dab2* ^{pd1162} larvae before onset of feeding (5 dpf) and after being fed with a non-calorie restricted SD (30 dpf). Growth deficits largely occur post-embryonically. **(E)** Intestine cross section images of 10 dpf *dab2* ^{pd1162} *+/−* or −/− larvae raised under non-calorie restricted SD. Arrowheads point to 4E8 colocalization with

phallodin, indicating no polarization defect in some of the *dab2 −/−*. L=lumen. n≥ 15 animals/genotype. Scale bar = 20 μm. * $p<0.05$, **** $p<0.0001$; two-tailed unpaired *t*-tests (A-C).

Author Manuscript Author Manuscript Author Manuscript Author Manuscript

Author Manuscript
Author Manuscript
Author Manuscript
Author Manuscript

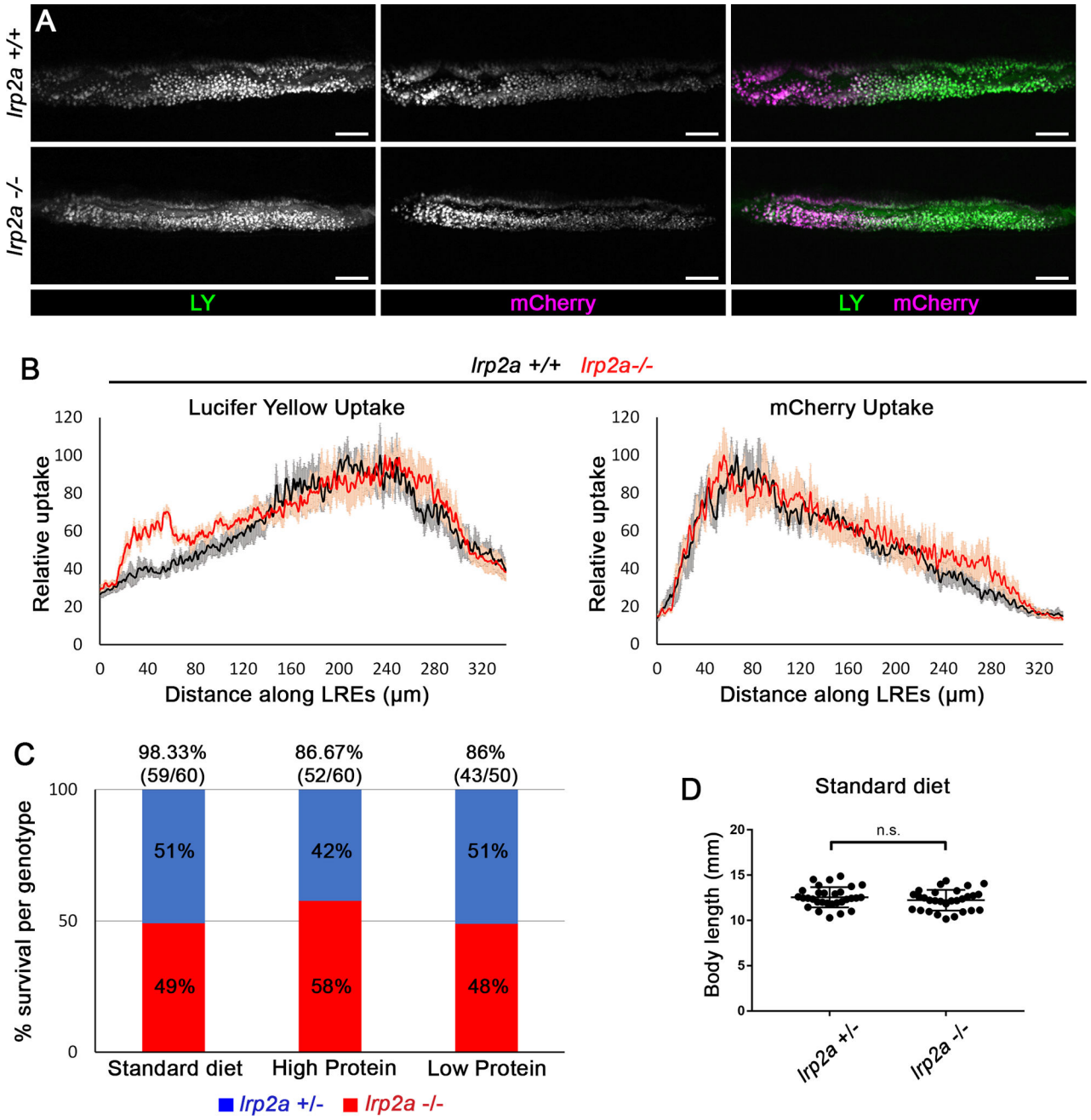

Figure 6. *lrp2a (megalin)* mutants do not show defects in LRE uptake or survival under different feeding conditions.

(A) Live confocal images showing LY or mCherry uptake in LREs of *lrp2a*^{mw1} *+/+, −/−* 6 dpf larvae. The larvae were imaged 5 hours after gavage. Scale bar = 20 μm. **(B)** Internalization profiles of LY (Left) and mCherry (Right) along LREs of 6 dpf *lrp2a*^{mw1} *+/+* (n=5), −/− (n=5). Data are means ± S.E.M. **(C)** Survival rates of *lrp2a*^{mw1} *+/−* and −/− 30 dpf larvae rasied under different feeding conditions: non-calorie restricted standard diet (SD), calorie-restricted high-protein diet (HP) and calorie-restricted low-protein diet (LP). Larvae from the cross *lrp2a*^{mw1} *+/−* X *lrp2a*^{mw1} −/− were used for the experiment. At 30 dpf, the survived larvae were counted and genotyped to determine what percentage of

Author Manuscript Author Manuscript Author Manuscript Author Manuscript

survived larvae are *lrp2a* +/− or −/−. The numbers above the graph bars indicate the percentage of overall tank survival for each feeding condition. **(D)** Comparison of body lengths of *lrp2a*^{mw1} +/− (n=30) and −/− (n=29) 30 dpf larvae raised under standard feeding condition. Two-tailed unpaired *t*-test was used for statistical analysis.

Author Manuscript
Author Manuscript
Author Manuscript
Author Manuscript

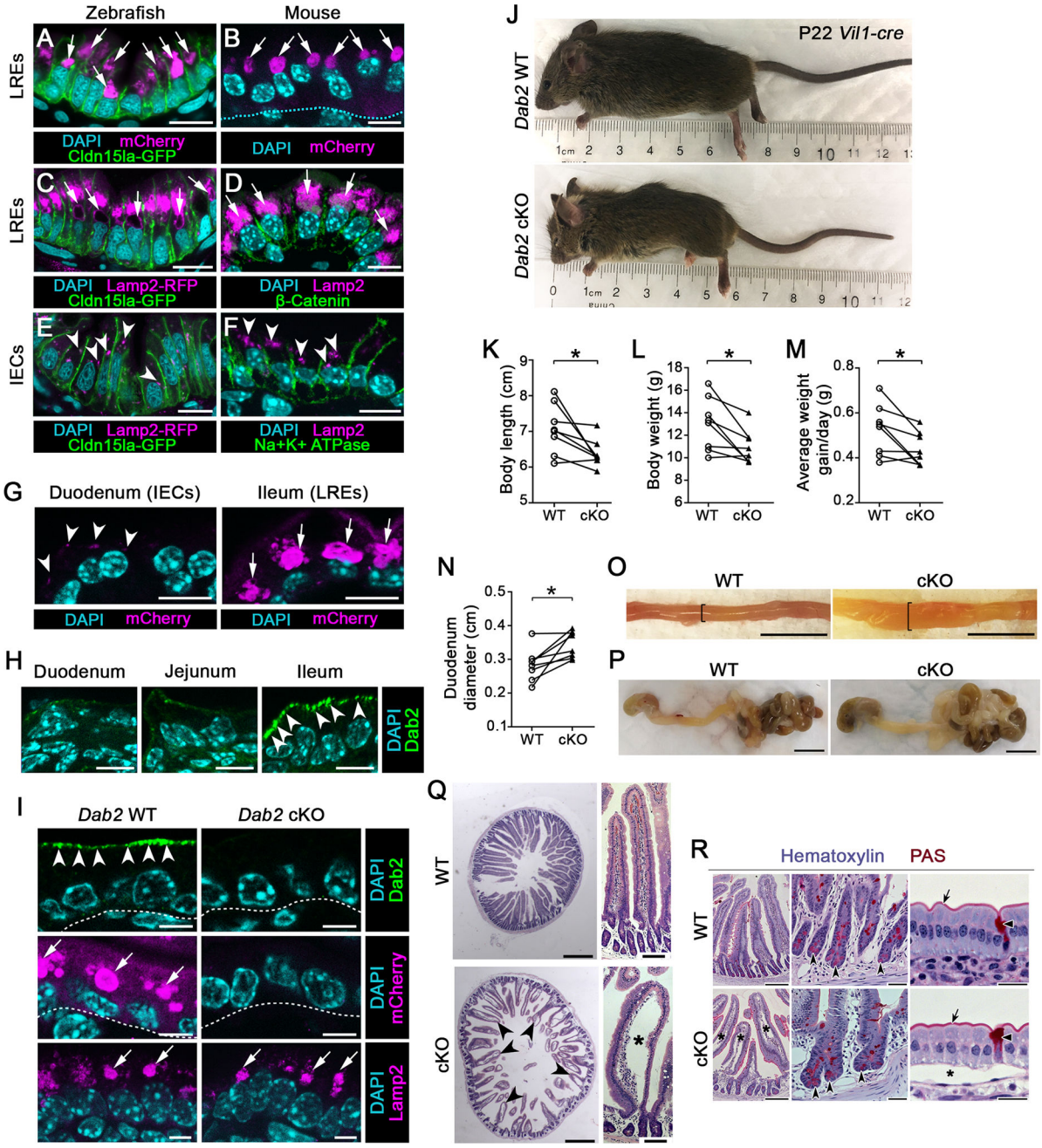

Figure 7. Loss of LRE function results in growth stunting and intestinal swelling in suckling mice.

(A, B) Confocal images of LREs of *TgBAC(cldn15la-GFP*^{pd1034}*)* zebrafish larva (A) and of P7 neonatal mouse (B) after mCherry uptake. Arrows point to lysosomal vacuoles filled with mCherry. Dashed line in (B) indicates basement membrane. Scale bar=10 μm. **(C-F)** Confocal images of LREs (C, D) and IECs (E, F) of *TgBAC(cldn15la-GFP*^{pd1034}*); TgBAC(lamp2-RFP*^{pd1044}*)* zebrafish larva and P7 neonatal mouse intestine stained with LAMP2 antibody, showing the presence of lysosomal vacuoles (arrows) in LREs (C, D) and lysosomes (arrowheads) in IECs (E, F). Scale bar=10 μm. **(G)** Confocal images of

Author Manuscript Author Manuscript Author Manuscript Author Manuscript

duodenum and ileum of P6 neonatal mouse after mCherry uptake. Arrowheads point to small vesicular structures with mCherry in IECs and arrows point to lysosomal vacuoles filled with mCherry in LREs. Scale bar = 10 μm. **(H)** DAB2 expression in the duodenum, jejunum, and ileum of P3 WT neonatal mouse. DAB2 expression is enriched in the ileum (arrowheads), the segment harboring LREs. Scale bar=10 μm. **(I)** mCherry uptake in the ileum of P6 *Dab2* WT and mCherry protein uptake (middle images; arrows) is abolished in *Dab2* cKO mouse ileal LREs, LAMP2 expression is not (bottom images; arrows). Scale bar=5 μm. **(J)** Images of P22 *Dab2* WT and *Dab2* cKO mice. **(K-N)** Quantitation of body length (K), weight (L), average weight gain/day (M), and duodenum diameter (N) of P22 *Dab2* WT and cKO mice. **(O)** Images of dissected duodenum of P22 *Dab2* WT and cKO mice. Brackets show prominent swelling of the GI tract in *Dab2* cKO mice. Scale bar=1 cm. **(P)** Images of the dissected stomach and intestinal tract of WT and Dab2 cKO mice harvested at P22. Scale bar=1 cm. **(Q)** Images of H&E stained sections of the duodenum of P22 *Dab2* WT and cKO mice, which exhibit severe distended villi (arrowheads and asterisk) indicative of submucosal edema. Scale bar=500 μm (transverse cross sections), 100 μm (longitudinal cross sections). **(R)** Hematoxylin and Periodic acid–Schiff (PAS) staining of duodenal sections of WT and Dab2 cKO P22 mice. Concave arrowheads point to Paneth cells within crypts; flat arrowheads show Goblet cells; arrows mark apical membrane; asterisks indicate edema. Scale bar= 200 μm (left), 40 μm (middle), 20 μm (right). In panels K-N, data points are littermate averages for each genotype and littermate averages of WT and cKO from the same litter are paired with lines. Measurements of individual mice from 8 different litters graphed in panels K-N are provided in the Table S2. * $p<0.05$; two-tailed paired *t*-tests (K-N). *p*-values, *t*-values and degree of freedom for the statistical tests are provided in the Table S3.

Author Manuscript Author Manuscript Author Manuscript Author Manuscript

KEY RESOURCES TABLE

REAGENT or RESOURCE	SOURCE	IDENTIFIER
Antibodies		
Rabbit polyclonal anti-Rab5	GeneTex	Cat# GTX13253
Rabbit monoclonal anti-Rab7 (D95F2)	Cell Signaling	Cat# 9367
Mouse monoclonal anti-Disabled-2/p96 (Clone 52/p96)	BD Biosciences	Cat# 610464
Mouse monoclonal anti-LAMP-2	DSHB	Cat# ABL-93
Chicken monoclonal anti-ATPase, (Na(+), K(+)) alpha subunit	DSHB	Cat# a5
Monoclonal anti-β-catenin (Clone 15B8)	Sigma-Aldrich	Cat# C7207
Anti-Zebrafish Gut Absorptive Cell Epitopes antibody [FIS 4E8/1]	Abcam	Cat# ab73643
Alexa Fluor™ 568 Phallodin	ThermoFisher	Cat# A12380
Chemicals, Peptides, and Recombinant Proteins		
Lucifer Yellow CH, Lithium Salt	ThermoFisher	Cat# L453
Transferrin From Human Serum, Alexa Fluor™ 488 conjugate	ThermoFisher	Cat# T13342
Dextran, Alexa Fluor™ 568; 10,000 MW	ThermoFisher	Cat# D22912
Lysotracker™ Red DND-99	ThermoFisher	Cat# L7528
BODIPY™ FL C16	ThermoFisher	Cat# D3821
SensiFAST™ SYBR® No-ROX Kit	Bioline	Cat# BIO-98005
Trypsin-EDTA	ThermoFisher	Cat# 25200056
Collagenase	Sigma-Aldrich	Cat# C2674
Propidium Iodide	ThermoFisher	Cat# P3566
BM-Purple	Roche	Cat# 11442074001
Critical Commercial Assays		
RNeasy Plus Micro Kit	Qiagen	Cat# 74034
Deposited Data		
Raw and analyzed data for RNA-seq experiment	This paper	GEO: GSE124970
Experimental Models: Organisms/Strains		
Zebrafish / *cubn*^{pd1169}	This work	N/A
Zebrafish / *dab2*^{pd1162}	This work	N/A
Zebrafish / *amn*^{pd1189}	This work	N/A
Zebrafish / *Tg(cldn15la:QF2)*^{pd1142}	This work	N/A
Zebrafish / *Tg(QUAS:GFP-Rab32a)*^{pd1201}	This work	N/A
Zebrafish / *Tg(QUAS:mCherry-snx27a)*^{pd1177}	This work	N/A
Zebrafish / *Tg(hsp:Venus-FYVE)*^{pd1046}	(Ellis et al., 2013)	N/A
Zebrafish / *Tg(hsp:laGFP)*^{pd1205}	This work	N/A
Zebrafish / *Tg(2.3k ifabp:sNgly-RFP)*^{pd1206}	This work	N/A
Zebrafish / *lrp2a*^{mw1}	(Veth et al., 2011)	N/A
Zebrafish / *TgBAC(cldn15la-GFP)*^{pd1034}	(Alvers et al., 2014)	N/A

Author Manuscript Author Manuscript Author Manuscript Author Manuscript

REAGENT or RESOURCE	SOURCE	IDENTIFIER
Zebrafish / *TgBAC(lamp2-RFP)*^{pd1044}	(Rodriguez-Fraticelli et al., 2015)	N/A
Zebrafish / *TgBAC(anxa2b-RFP)*^{pd1113}	(Marjoram et al., 2015)	N/A
Mouse / Villin-Cre	(el Marjou et al., 2004)	N/A
Mouse / Villin-CreER	(el Marjou et al., 2004)	N/A
Mouse / Dab2$^{fl/fl}$ (B6; 129S4-*Dab2*^{tm1Cpr}/J)	Jackson Laboratory (Morris et al., 2002)	Cat# JAX:022837; RRID:IMSR_JAX:022837
Oligonucleotides		
Primers for cloning pME-DN-Dab2: forward: 5' CCACTCACCATGACTGCACCCGTGACCAG 3'	This work	N/A
Primers for cloning pME-DN-Dab2: reverse: 5' CTTTTGTCCAGCCTCCTGCTC 3'	This work	N/A
Genotyping primers for *cubn*^{pd1169}: forward: 5' ACTCTGTTCACCTGCAGTGC 3'	This work	N/A
Genotyping primers for *cubn*^{pd1169}: reverse (DCAPS): 5' TGACATCCGAGTGGAGTTCCTGCCAAGAC 3'	This work	N/A
Genotyping primers for *dab2*^{pd1162}: forward: 5' ACAGACGAGTTCCTCTTGGC 3'	This work	N/A
Genotyping primers for *dab2*^{pd1162}: reverse, 5' CCGCTTCTTGCAGTGCTAGA	This work	N/A
Genotyping primers for *amn*^{pd1189}: forward: 5' GGATGAGCTTGCCTGTGGAT 3'	This work	N/A
Genotyping primers for *amn*^{pd1189}: reverse, 5' GAATGAGGTGGCGTCTCGAA 3'	This work	N/A
Primers for generating in situ probes for *dab2* and *amn*, see Table S4	This work	N/A
Recombinant DNA		
p5E-QUAS	(Subedi et al., 2014)	N/A
p5E-cldn15la	(Murdoch et al., 2019)	N/A
pME-QF2	(Subedi et al., 2014)	N/A
pME-DN-Dab2	This work	N/A
pRSETB-mCherry	(Sarabipour et al., 2014)	N/A
pRSETB-mTurquoise	(Sarabipour et al., 2014)	N/A
pGEMTeasy-lrp2a	(Anzenberger et al., 2006)	N/A
pCR TOPO-cubilin	(Anzenberger et al., 2006)	N/A
Software and Algorithms		
DAVID Bioinformatics Resources 6.8	(Huang da et al., 2009a, b)	https://david.ncifcrf.gov/
DESeq2	(Anders et al., 2015; Love et al., 2014)	https://usegalaxy.org/root?tool_id=toolshed.g2.bx.psu.edu/repos/iuc/deseq2/deseq2/2.11.39
htseq-count	(Kim et al., 2015)	https://usegalaxy.org/root?tool_id=toolshed.g2.bx.psu.edu/repos/lparsons/htseq_count/htseq_count/0.6.1galaxy3

Author Manuscript

Author Manuscript

Author Manuscript

Author Manuscript

REAGENT or RESOURCE	SOURCE	IDENTIFIER
HISAT2	(Kim et al., 2015)	https://usegalaxy.org/root?tool_id=toolshed.g2.bx.psu.edu/repos/iuc/hisat2/hisat2/2.0.5.2
Graphpad Prism	GraphPad Software, La Jolla, CA, USA	https://www.graphpad.com/scientific-software/prism/; RRID: SCR_002798